DESIGNING A CHEST PULSE OXIMETER TO MEASURE BLOOD OXYGEN LEVEL

by
Surhan Bozkurt

Submitted to Graduate School of Natural and Applied Sciences
in Partial Fulfillment of the Requirements
for the Degree of Master of Science in
Electrical and Electronics Engineering

Yeditepe University
2015

DESIGNING A CHEST PULSE OXIMETER
TO MEASURE BLOOD OXYGEN LEVEL

APPROVED BY:

Assist. Prof. Dr. Gökhan Ertaş ……
(Thesis Supervisor)

Prof. Dr. Ali Ümit Keskin ……

Prof. Dr. Tülay Yıldırım ……

DATE OF APPROVAL: …./…./2015

ACKNOWLEDGEMENTS

It is with immense gratitude that I acknowledge the support and help of my supervisor Dr.Gökhan Ertaş. Pursuing my thesis under his supervision has been an experience which broadens the mind and presents an unlimited source of learning.

I would like to express my sincere thanks appreciation to Cenap Turan, Sinan Yağcıoğlu, Hakan Bozkurt, Betül Yardibi, Mehmet Nacar and all my students who help me during my MSc study.

Finally, I would like to thank my family for their endless love and support, which makes everything more beautiful.

ABSTRACT

DESIGNING A CHEST PULSE OXIMETER TO MEASURE BLOOD OXYGEN LEVEL

Nowadays, the biomedical devices hold a prominent position within medicine. Pulse oximeter has become a significant tool to detect oxygen level in blood. This measurement can be performed from different sites of human body such as fingertip, forehead, earlobe and nose. However, medical doctors agree that any SpO_2 measurement should be better performed from sites closer to the heart in order to detect some diseases in their early stages.

In this study, a reflective sensor was designed and SpO_2 estimations were carried out from right index fingertip and intercostal artery in center of left chest and then, the results were compared. In this device, the sensor capture red and infra-red light that comes from related area from human body and produces an analog signal. The captured signal was amplified, filtered, digitized and sent to Personal Computer to process by using several digital windows namely Hamming, Blackman, Bartlett, Digital Prolate Spheroidal Sequence, Kaiser and Parzen-Rosenblatt. SpO_2 estimations were obtained from related calibration equation for each window output. These equations were obtained from measurements of eight healthy volunteers. Another group of twenty-one healthy volunteers are included into the study while obtaining SPO_2 estimations from right index fingertip and from the intercostal artery in the center of the left chest. The average SpO_2 estimated from chest photoplethysmograms are 95.87±0.26, 95.88±0.26, 95.93±0.64, 95.75±0.36, 95.84±0.32 and 95.78±0.28 for Digital Prolate Spheroidal Sequence, Hamming, Kaiser, Blackman, Bartlett and Parzen-Rosenblatt windows, respectively. The average SpO_2 estimated from fingertip photoplethysmograms are 96.15±0.29, 96.15±0.25, 95.70±0.40, 96.07±0.35, 96.12±0.41 and 96.13±0.31 for DPSS, Hamming, Kaiser, Blackman, Bartlett and Parzen-Rosenblatt windows, respectively. The results show that, there is no systematic difference between SpO_2 estimations from chest and fingertip ($P<0.5$).

ÖZET

KANDAKİ OKSİJEN SEVİYESİNİ ÖLÇMEK İÇİN BİR GÖĞÜS PULSE OKSİMETRESİ TASARIMI

Günümüzde biyomedikal cihazlar tıpta önemli bir yer tutmaktadır. Pulse oksimetre kandaki oksijen seviyesini belirlemede önemli bir araç haline gelmiştir. Bu ölçüm tekniği parmak ucu, alın, kulak memesi ve burun gibi vücudun değişik bölgelerinden gerçekleştirilebilmektedir. Yine de pek çok medikal doktor SpO_2 ölçümünüm bazı hastalıkların erken teşhisi için kalbe yakın gerçekleşmesi gerektiğini belirtmektedir.

Bu çalışmada, yansıtıcı tarzında bir SpO_2 algılayıcı tasarlanmış ve sağ işaret parmağı ucu ve sol göğüs bölgesinde intercostal atardamardan SpO_2 kestirimi gerçekleştirilmiştir ve daha sonra sonuçlar karşılaştırılmıştır. Bu cihazda, algılayıcı vücudun ilgili bölümünden gelen kırmızı ve kızılötesi ışığı yakalar ve analog bir işaret üretir. Yakalanan sinyal kuvvetlendirildi, filtrelendi, sayısala çevrildi ve çeşitli sayısal pencereler kullanılarak işlenmek için bilgisayara gönderildi. Kullanılan pencereler Hamming, Blackman, Bartlett, Digital Prolate Spheroidal Sequence, Kaiser ve Parzen-Rosenblatt perncereleridir. Her bir pencere çıkışı için, SpO_2 kestirimi ilgili kalibrasyon denklemi kullanılarak elde edilmiştir. Bu denklemler sekiz sağlıklı gönüllüden alınan ölçümlerden elde edilmiştir. Diğer yirmi bir kişiden oluşan grup sağ işaret parmağı ve sol göğüste yer alan intercostal atardamardan alınan SpO_2 kestirimlerini içermektedir. Göğüs photopletysmogramlarından ortalama SpO_2 kestirimleri sırasıyla DPSS Hamming, Kaiser, Blackman, Bartlett ve Parzen-Rosenbaltt pencereleri için göğüste 95.87±0.26, 95.88±0.26, 95.93±30.64, 95.75±0.36, 95.84±0.32 95.78±0.28 ve parmak photopletysmogramlardan SpO_2 kestirimleri Digital Prolate Spheroidal Sequence, Hamming, Kaiser, Blackman, Bartlett ve Parzen-Rosenbaltt pencereleri için sırası ile 96.15±0.29, 96.15±0.25, 95.70±0.40, 96.07±0.35, 96.12±0.41 ve 96.13±0.31. İstatistik analizi sonuçları bize parmak ve göğüs için SpO_2 kestirimleri arasında sistematik bir fark olmadığını göstermektedir ($P<0.5$).

TABLE OF CONTENTS

LIST OF FIGURES

LIST OF TABLES

LIST OF SYMBOLS/ABBREVIATIONS

A_λ	Absorbent at wavelength λ
c	Concentration of absorbent
$e_{calibration}$[%]	Calibration error
$e_{calibrated\ oximeter}$	Calibrated oximeter error
$e_{reference\ oximeter}$	Reference oximeter error
f	Frequency
h	Scaling Factor
I	Light Intensity
I_0	Incident Light Intensity
I_{max}	Maximum light intensity
I_{min}	Minimum light intensity
l	Optical path length
n	Sample number
N	Window size
y_i	Measurement a data points
$\hat{y}_i$	i^{th} SpO_2 value from calibrated device
ε_λ	Extinction Coefficient
λ	Wave length
DPSS	Digital Prolate Spheroidal Sequence
SpO_2	Oxygen Saturation
PPG	Photoplethysmogram
RR	Ratio of two differential absorption with different wave length

1. INTRODUCTION

Many biological process is depend upon the oxygen. In human body, hemoglobin is responsible for oxygen transportation. Therefore, amount of oxygen level is very significant in the blood and obtain critical medical information.

The respiratory system includes lungs, conducting airways that direct air to the gas exchange sites, part of the central nervous system muscle of chest wall and diaphragm that are responsible for inflation and deflation of the lungs. The lungs fill most of the thoracic cavity expect for the space occupied by the heart and blood vessels [1].

Body cells need oxygen to perform aerobic respiration. Oxygen transportation is performed through the circulatory system. Deoxygenated blood enters to right side of the heart where it is pumped to the lungs to be oxygenated. When blood goes the pulmonary alveoli where gas exchange occurs [1].

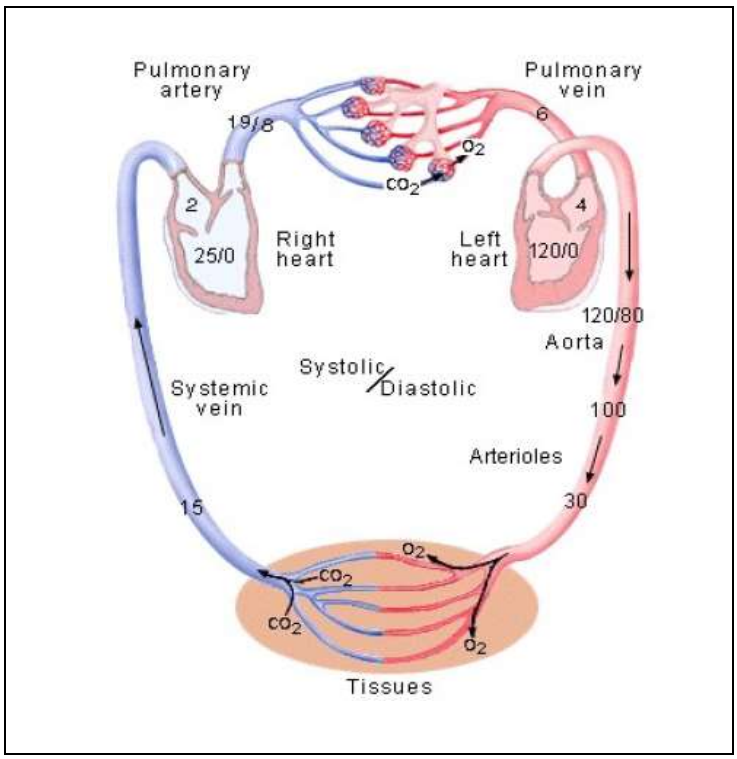

Figure 1.1. Respiratory physiology [2]

1.1. BEER-LAMBERTS LAW

Measurement of the oxygen concentration in blood is based on Beer-Lambert Law that describes light attenuation through a sample homogenous non-scatting media using [3]

$$I = I_0 e^{-\varepsilon_\lambda c l} \tag{1.1}$$

here I, I_0, ε_λ, λ, c, l represent, transmitted intensity of the light, the incident intensity, the extinction coefficient, wave length, the concentration of the absorbent and optical path length of sample, respectively. If there exist different layers, total intensity of transmitted light is used and the general equation becomes

$$I = I_0 e^{\sum -\varepsilon_\lambda c_a l_a} = I_0 e^{-A} \tag{1.2}$$

here absorbance, A at wavelength λ is defined as the negative natural logarithm of the fraction of light that passes through a sample:

$$A_\lambda = -\ln\left(\frac{I}{I_0}\right) = \sum_a \varepsilon_{\lambda,a}\, c_a l_a \tag{1.3}$$

When pulse oximetry is considered, the DC component of transmitted light (signal) is defined as the transmission without pulsation. AC component of the transmitted signal is time-dependent arterial pulsation of the transmission signal [3].

$$d(A_\lambda) = \frac{d(A_\lambda)}{dt} \cdot \Delta t = \frac{dl_{art}}{dt} \cdot \sum \varepsilon_{\lambda,art} \cdot c_{art} \cdot \Delta t \tag{1.4}$$

where I_{art} represents as path length through arterial blood. On the other hand, differential absorption can be written by using transmitted intensities [3].

$$d(A_\lambda) = \frac{AC_\lambda}{DC_\lambda} = \frac{I_{max} - I_{min}}{I_{min}} \tag{1.5}$$

where I_{min} and I_{max} represent minimum transmitted light intensity after systolic raise and maximum transmitted light intensity after diastolic raise, respectively. Considering absorption spectrum of oxy- and deoxy-hemoglobin, in pulse oximetry, two different wavelengths emitted by red and infrared light emitting diodes have been used and a ratio, namely RR, is computed.

$$(RR) = \frac{d(A_{red})}{d(A_{ired})} = \frac{\left(\varepsilon_{HbO_2,red} \cdot c_{HbO_2} + \varepsilon_{RHb,red} \cdot c_{rHb}\right) \cdot \Delta l}{\left(\varepsilon_{HbO_2,ired} \cdot c_{HbO_2} + \varepsilon_{RHb,ired} \cdot c_{rHb}\right) \cdot \Delta l} \tag{1.6}$$

A more practical and direct way for RR calculation is the use of photoplethysmogram, a signal captured as a result of Beer-Lamberts Law from skin and the following equation [4].

$$(RR) = \frac{\log 10 \frac{I_{rAC}}{I_{rDC}}}{\log 10 \frac{I_{irAC}}{I_{irDC}}} \tag{1.7}$$

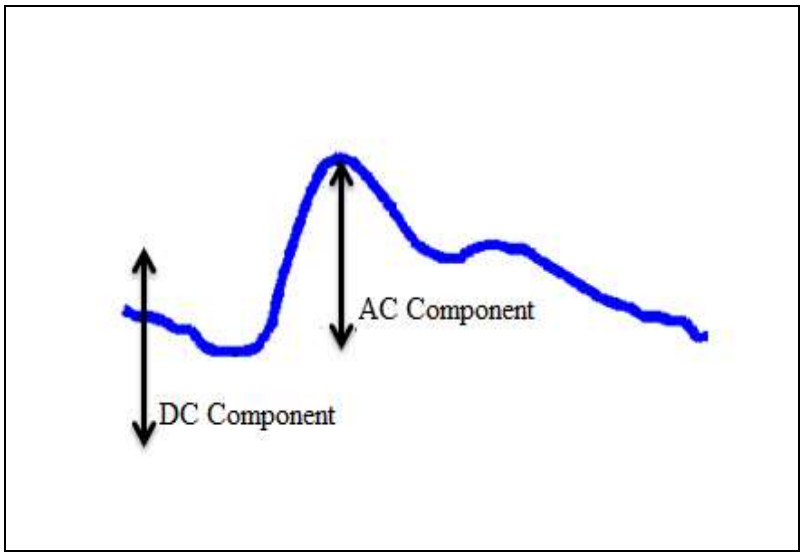

Figure 1.2. Photoplethysmogram and its AC component, I_{rAC} and its DC component, I_{rDC}

The principle of photoplethysmogram is based on red and infrared light absorption characteristics. As seen in Figure 1.3, oxygenated hemoglobin in blood absorbs more led light and allows more infrared light to pass. However, deoxygenated hemoglobin absorbs more infrared light and allows more red light to pass. The ratio of oxygenated to the total concentration of hemoglobin in the blood is terms as SpO_2 which is found from the RR ratio using [5]:

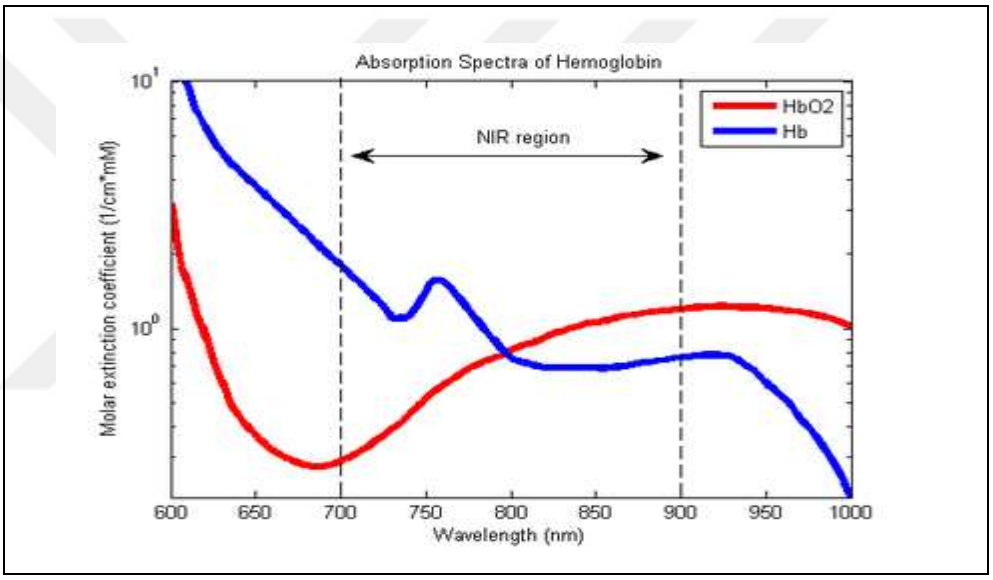

Figure 1.3. Absorption spectrum of oxygenated hemoglobin (HbO_2) and deoxygenated hemoglobin (Hb) in blood [6]

1.2. PULSE OXIMETRY

Pulse oximeters consist of two light sources (red and infrared), a phototransistor to detect absorption of the light source, an analog filter to minimize noise and a microprocessor unit to calculate heart rate and estimate RR and consequently SpO_2 percentage [7]. Medical use of pulse oximeters are widespread [8]:

- During anesthesia and post anesthesia care, including both general and conscious sedation. If SpO_2 value is too little or ventilation fails, an alarm sounds.
- Intensive care units.
- Neonatal care units, including delivery, nursery and neonatal intensive care unit. SpO_2 value is taken immediately taken from right hand after birth within five minutes. If SpO_2 value is too little or too high, It is dangerous for neonate.
- Hospital medical unit.
- Transportation within the hospital during ambulance or air ambulance transportation.
- Diagnosing testing, such as pulmonary function testing, exercise testing and during sleep studies.
- Sub-acute care centers, such as nursing homes and rehabilitation centers.
- Home care patients.

There are three types of SpO_2 measurement techniques in clinical practice [9]:

- Invasive fiber optic oximeter to measure arterial and intra cardiac oxygen saturation.
- In vitro examination of arterial blood sample to measure oxygen saturation.
- Non-invasive oximeter to monitor arterial oxygen saturation.

The fiber optic oximeter, invented by Michael Polonyi in 1960 [10], had been used in cardiac surgery. Simon and Clark reported that invasive oxygen saturation measurement decreases the need for arterial gas analysis by 37% and causes the significant changes in the medical treatment [11]. This lead to new developments in non-invasive oxygen saturation measurement techniques. The first non-invasive pulse oximeter was invented by Takuo Aoyagi in 1974. This instrument used by Nakajima and his associates [12]. Pulse oximeter device, which is measured for ear, was invented by Robert Shaw who is surgeon in San Francisco. This device uses eight wavelength to identify the separate Hb species therefore is quite expensive but accurate down to %70 SaO_2 [10].

Some studies focus to investigate the accuracy of the different probes that used for SpO_2 devices. There are SpO_2 devices designed in order to measure oxygen saturation from the toe, fingertip, ear lobe, nose and forehead [13]. The forehead sensor was developed by Nellcor. This sensor would not be affected by patient movements and would yield the best

performance under low temperature. MacLeod showed that forehead probe responded faster than probes in 2005 [14]. Mannheimer and Bebout reported that forehead probes have significant advantages over the finger probes [15]. Juban reported that finger probes had lower precision in patients with poor peripheral perfusion in 1999. Fernandez suggested that in patient with low cardiac index, the forehead probe was better than the digit sensor for SpO_2 devices [16]. The forehead probes place nearer region to heart in human body according to finger probes so that forehead probes can detect the hypoxia faster [17].

Figure 1.4. SpO_2 measurement form fingertip [18]

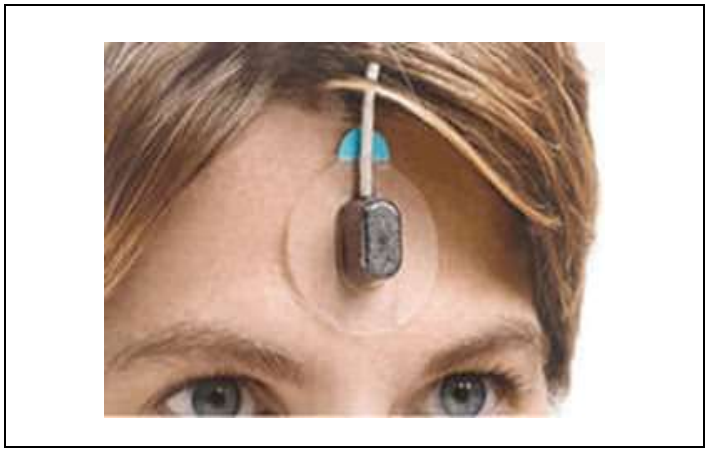

Figure 1.5. SpO_2 measurement from forehead [19]

Figure 1.6. SpO_2 measurement from earlobe [20]

Figure 1.7. SpO_2 measurement from nose [21]

Figure 1.8. SpO_2 measurement from chest

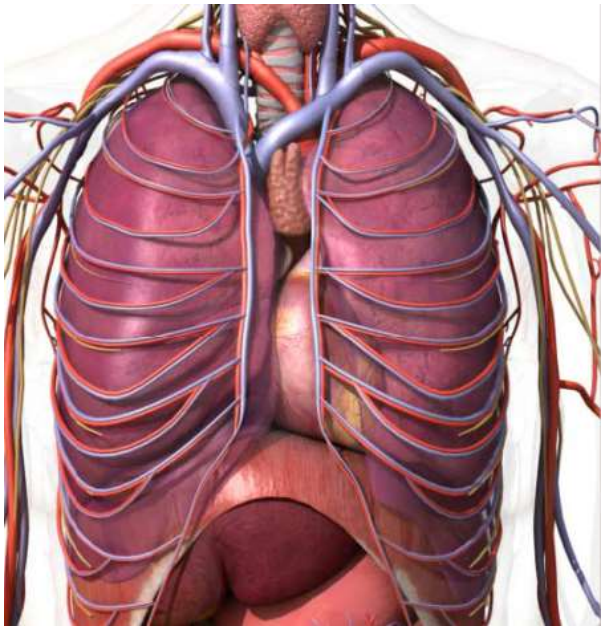

Figure 1.9. Intercostal artery in human body

There are two different type sensor for the pulse oximeter device (reflective and transmissive sensors). Reflective sensor consists of red and infrared LEDs and a phototransistor that is placed beside of the LEDs. SpO_2 measurements can be taken from fingertip, forehead, wrist and nose using reflective pulse oximeter sensor. Transmissive sensor consists of red and infrared LEDs and a phototransistor that is placed of the opposite side of the LEDs. SpO_2 measurement can be taken from fingertip and ear lobe using transmissive pulse oximeter sensor.

Figure 1.10. Transmissive SpO_2 sensor

1.3. RECENT STUDIES ON PULSE OXIMETER

Studies on pulse oximeters focus on sensor design, reliable signal acquisition and processing technique and accurate SpO_2 estimation.

Pank et al. [22] presented a ring type pulse oximeter finger sensor and a 24 hour ambulatory heart rate monitoring system for the aged. They designed the sensor using a microprocessor with a built-in ZigBee stack. They also analyzed the distorted signal using fast Fourier transform and designed an algorithm using least square estimator to calibrate

signal. Baherati et al. [23] presented an ultralow power pulse oximeter sensor for long term measurements. They describe a compressed sensing approach to sample the photodetector output. LEDs can turned off for longer periods and save sensor power. Xiaoying et al. [24] designed a reflectance pulse oximetry measurement system using the MSP430F149 microcontroller. This microcontroller has ultralow power capability making the system power consumption is quite low. Nogava et al. [25] developed of a reflectance SpO_2 sensor for broader clinical application to measure from different human body regions. The new reflectance pulse oximeter sensor has improved linearity over the broader SpO_2 range from 100% to 30%. Results show that closer wavelengths for red and infrared signals give better results. LED driving currents can be reduced significantly by increasing the active area of the photo detector in the reflectance pulse oximeters. Ogino et al. [26] designed a multi reflective SpO_2 sensor system to measure physiological data about human stress or fatigue condition from ear lobe, mouth and finger. The elastic gum optical shield and the reflective optical shield were used to improve a fit of the sensor and increase pulsatile signal component of PPG signal. Results show that reflectance SpO_2 sensor has better correlation with transmittance SpO_2 sensor placed on ear lobe. SpO_2 measured from maxilla indicates oxygen supply to brain. SpO_2 sensor is available to measure SpO_2 from mouth. Schreiner et al. [27] proposed a chest-based SpO_2 system. The system was optimized through adjustment of optical component alignment and through fine-tuning of LED intensity and receiver sensitivity. Results show that chest based SpO_2 measurements require high illumination of the tissue, large feedback gain and high order filters. Fuke et al. [28] developed a prototype of small wearable device consisting of electrocardiogram and Photoplethysmogram sensor to measure from chest. The results show that the system could sense tendency of time–dependent change of blood pressure by measuring pulse of vessel over the sternum while its propagation distance is short.

There are also some studies focus on filtering of the signals acquired (photoplethysmograms). Reddy et al. [29] developed a method for removing motion artefacts from corrupted photoplethysmograms by applying Fourier series analysis on a cycle by cycle basis is presented. The results show that the method is insensitive to heart rate variation, introduces negligible error in the processed photoplethysmograms due to the additional processing, preserves all the morphological features of the Photoplethysmogram and provides 35dB reduction in motion artefacts. Seedtabaii et al. [30] presented a study on

using Kalman Filter in an innovative way by modelling both the artillery blood pressure and unwanted signal, additive motion, artefact, to reduce motion artefacts from corrupted photoplethysmograms. The results show that acceptable performance. Kim et al. [31] proposed an adaptive noise cancellation method to obtain the accurate physiological signal in the situation where the little movement is allowed. Photoplethysmogram were recorded from forehead during in motion and calibrated using the motion signal. The results show that the calibrated Photoplethysmogram is accurate enough by comparing with the results that is measured at the finger without movement. Lee et al. [32] propose periodic moving average filter to remove motion artefacts. This method is based on the quasi-periodicity of the photoplethysmograms. After segmenting the photoplethysmogram on periodic boundaries, the signal is averaged the m^{th} samples of each period. The results show that motion artefacts are removed well without the deterioration of the characteristic point.

Pilt et al. [33] proposed adaptive sum comb filter to detect AC component of the Photoplethysmogram. The results show that adjusted comb filter has about 7dB better noise attenuation than non-adjusted comb filter using same number of recurrences for filter output cancellation. Lee et al. [34] proposed adaptive comb filter to reduce motion artefact effects from photoplethysmograms. The results show that adaptive comb filter with adaptive lattice infinitive impulse response notch filter successfully reduces motion artefacts from the quasi-periodic Photoplethysmogram. Ram et al. [35] presented an adaptive filtering method technique Time Varying Step-size Least Mean Square filter to reduce motion artefact effect. This method lies in the fact that synthetic noise reference signal for adaptive filtering, representing motion artefact noise, is generated internally from the motion artefact corrupted photoplethysmogram itself instead of using any additional hardware such as accelerometer or source-detector pair for noise reference signal generation. The results show that on the PPG data recorded with different motion artefacts, demonstrated the efficacy of the proposed Time Varying Step-size Least Mean Square algorithm in motion artefacts reduction.

Lee et al. [36] proposed a particle filtering method and this algorithm shows to effectively to reduce the movement noise and improve emotion recognition accuracy absolutely by 12.7% and 10.9% in the situations where users move arms and walk on a road, respectively. The results show that the algorithm improved output Signal to noise ratio (SNR) than conventional normalized least mean square by 4.5 dB on average in the same

situation. Yuliang et al. [37] proposed a filtering method based on wavelet transform combined with adaptive filter to eliminate motion artefacts. This method extracts the motion artefact using wavelet transform. The results show that this method can effectively remove motion artefact and improve the signal quality. Naraharisetti et al. [38] gave five different methods to reduce motion artefacts which include Adaptive Noise Cancellation, Wavelet Transform, Independent Component Analysis, Singular Value Decomposition and Cycle by Cycle Fourier Series Analysis. The results show that after implementing five methods revealed that Singular Value Decomposition and Fourier Series Analysis Method gives better results in terms of artefact reduction and signal restoration. Scharf et al. [39] used analog filter and moving average method to filtering SpO_2 signals. This study evaluated spectral analysis to obtain SpO_2 signals using Fast Fourier Transform. SpO_2 value was computed using magnitude of the peak in the cardiac spectrum. Lee et al. [40] presented three method to detect respiratory rate. PPG signal was generated using a commercial device to analyze Min-Max, Peak to Peak and Pulse shape of the signal. Results show that Min-Max and Peak to Peak performed better that Pulse shape. This methods is alternative to detect respiratory rate. Becerra-Luna et al. [41] presented Adaptive Noise Canceller using averaged least squares algorithm to reduce miokinetic nose attenuation. 12 volunteer were used to record PPG signal with miokinetic noise during one minute. Results show that miokinetic noise attenuation of the PPG signal, which could be used when the PPG records are contaminated with sudden movements, the average error between the PPG signal recovered by the filter and the PPG without noise miokinetic in percentage terms was 11.5% Yang et. al [42] adopted the Fourier Analysis method to perform noise cancellation from PPG signals. Noise cancellation is major issue to calculate SpO_2 value. Magnitude of the PPG signal have significant role to calculate SpO_2. Results show that Fourier analysis available method to noise cancellation. This algorithm performs PPG signal acquisition, motion artefact reduction and SpO_2 calculation. Shafgat et al. [43] presented a 776^{th} order finite impulse response (FIR) filter and a 695^{th}order interpolated finite impulse response (IFIR) filter to reduce artefacts from lower esophagus. Results show that the IFIR filter was better since it conformed more closely to the desired filter specifications and allowed real-time processing. The average improvement of the signal to noise ratio (SNR) achieved by FIR and IFIR filters fundamental component of the red signal with respect to fundamental component of the artefact were 57.96 and 60.60dB, respectively and for the infrared PPG signals were 54.83

and 60.96 dB. These filter were also compared with 10^{th} order Butterworth filters. The average SNR improvement of the FIR and IFIR filters was significantly higher than Butterworth filter.

There are also some studies focuses on the designing new SpO_2 devices. Dai et al. [44] design a non-invasive SpO_2 measurement device and the method of near infrared spectroscopy measurement, a wireless SpO_2 device was designed with the use of Bluetooth 4.0 technology, combining smart mobile APP with hardware. This device use radio frequency integrated chip CC2540 to control LEDs. This system calculates the SpO_2, pulse rate and draws the PPG signal. Result show that the system feasibility of the system verified through practical test. Kollman et al. [45] present a novel SpO_2 device based on low power, low cost and Vertical Cavity Surface Emitting Laser (VCSEL) technology. This system can help address a need to perform regular measurements of SpO_2 device for patients with chronic obstructive pulmonary disease. The VCSELs were integrated into a SpO_2 device that is unobtrusive and suitable for long term wearable use. The results show that the prototype achieved good performance and can be worn behind the ear like a hearing aid. Li et al. [46] present a small and low-cost SpO_2 device. Unfiltered PPG signals were digitalized and directly digital filters were used for signal extraction and noise reduction. The result show that, in high-fidelity PPGs with thousands of peak to peak digitalization levels that are sampled at 240 Hz to avoid noise aliasing. Electronic feedback controls make the PPG signals more resilient in the face of the environmental changes. Ateş et al. [47] designed a SpO_2 system and calibrated the system using calibration curve. Linear regression used to extract relation between R and SpO_2. Then Fuzzy Logic used to calculate SpO_2. Results show that Fuzzy Logic gives more reliable and healthy results. Peterson et al. [48] presented a conventional SpO_2 device measures form finger with a mobile phone through head jack audio interface. PPG signals processed using audio sub system of phone. Results show that audio SpO_2 system gives consistent and good results. Kock et al. [49] proposed to exploit the unique transparency of the ocular media to make reflectance SpO_2 device on the retinal fundus. An in vitro system developed to simulate retinal circulation and ocular optics. The system consists of a flexible cuvette located in the model eye and blood circulation to simulate arterial blood flow. Results show that cardiac synchronous signal can be detected from retina using retinal SpO_2 device. Potuzakova et al. [50] proposed a reflective SpO_2 device based on Near Infrared Spectroscopy technique

will be more comfortable use in long term monitoring. Reflective sensor embedded in the soft foam and fabric materials built more comfortable. Results show that signal quality on the different body locations is reported and questionnaires for comfort assessment are analyzed.

1.4. LIMITATIONS OF PULSE OXIMETERS

There are several conditions that have undesirable impact on SpO_2 measurements. For instance, if the perfusion is decreased, the pulse amplitude will get smaller leading to error prone measurements. Poor perfusion, as a result of cold or hypertension, leads to poor quality photoplethysmograms with low signal-to-noise ratio that can be easily altered by artefacts. Motion artefacts can interfere with signal detection leading to unstable photoplethysmograms. Irregular cardiac rhythm, edema and venous congestion may also lead to inaccurate measurements. Carbon monoxide poisoning may also result erroneous SpO_2 measurements as a result of carboxyhemoglobin. Smokers often have high readings after smoking since cigarettes contain carbon monoxide.

SpO_2 measurement is significant research area to improve measurement accuracy. Measurement accuracy can be increased to take measurement form the nearest region of the heart and diagnoses can be also detected in early stage. Main focus of this study, designing a pulse oximeter system to measure SpO_2 from the intercostal artery in the center of the left chest.

2. MATERIALS AND METHODS

In this study, a chest pulse oximeter system has been developed to estimate oxygen level in blood from chest. The block diagram of the system is as seen in Figure 2.1. In brief, red and infrared LEDs are lighted in an order determined by a predefined sequence. The light reflected by the relevant human tissue is captured by the phototransistor. The output signal from the phototransistor is filtered, amplified, digitized and next transferred to the personal computer. On the computer, digital filtering with different windows are applied to the digital data received and finally SpO2 estimation is obtained.

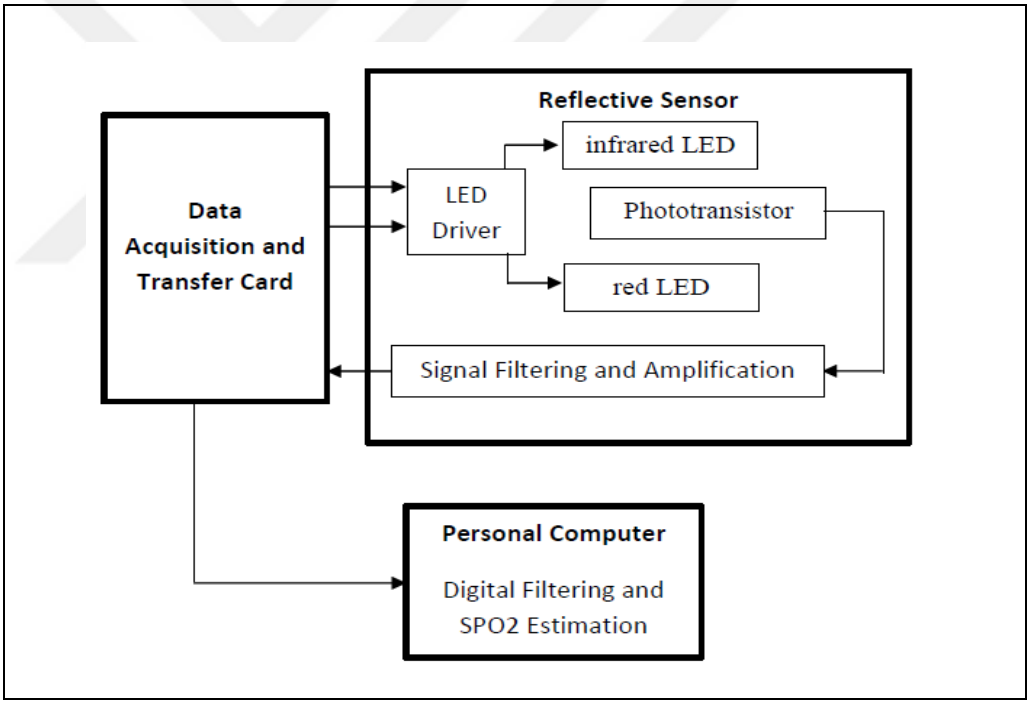

Figure 2.1. Block diagram of the pulse oximeter developed

2.1. REFLECTIVE SENSOR

In this study, a reflective sensor has been designed to capture Photoplethysmogram signals. The electronic circuit, the printed circuit board and the physical design of the sensor are as

seen in Figure 2.2 The sensor is equipped with a red LED, an infra-red LED and a phototransistor. As shown in Figure 2.3, the peak wavelength of each LED is 660nm and 940nm, respectively., the phototransistor is Vishay BPW77NB [51] providing a spectral bandwidth ranging from 450 to1080nm and good relative radiant sensitivity as seen in Figures 2.4 and 2.5.

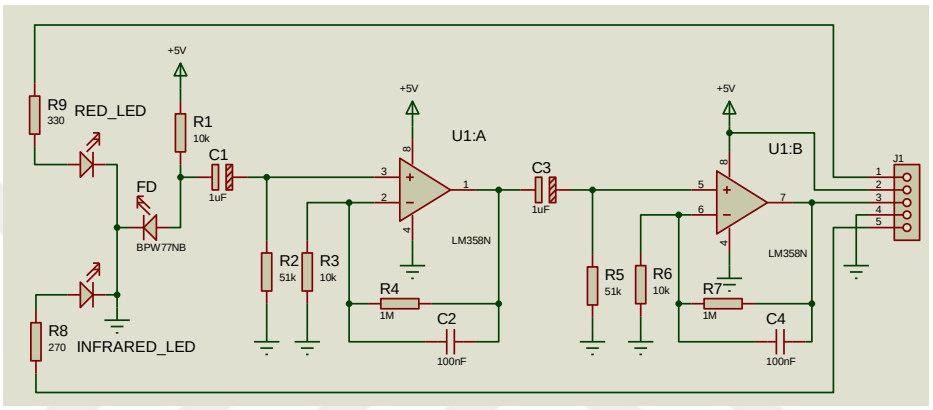

(a)

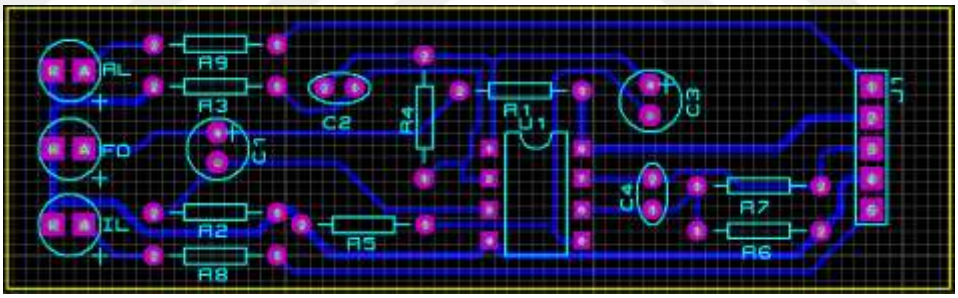

(b)

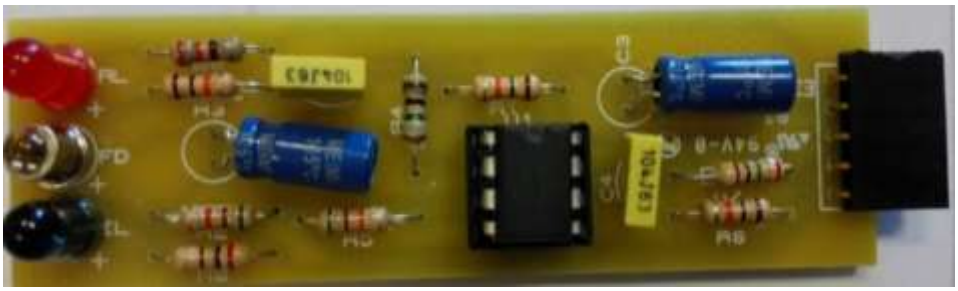

(c)

Figure 2.2. The reflective sensor developed: a) electronic circuit design, b) printed circuit board design and c) physical design

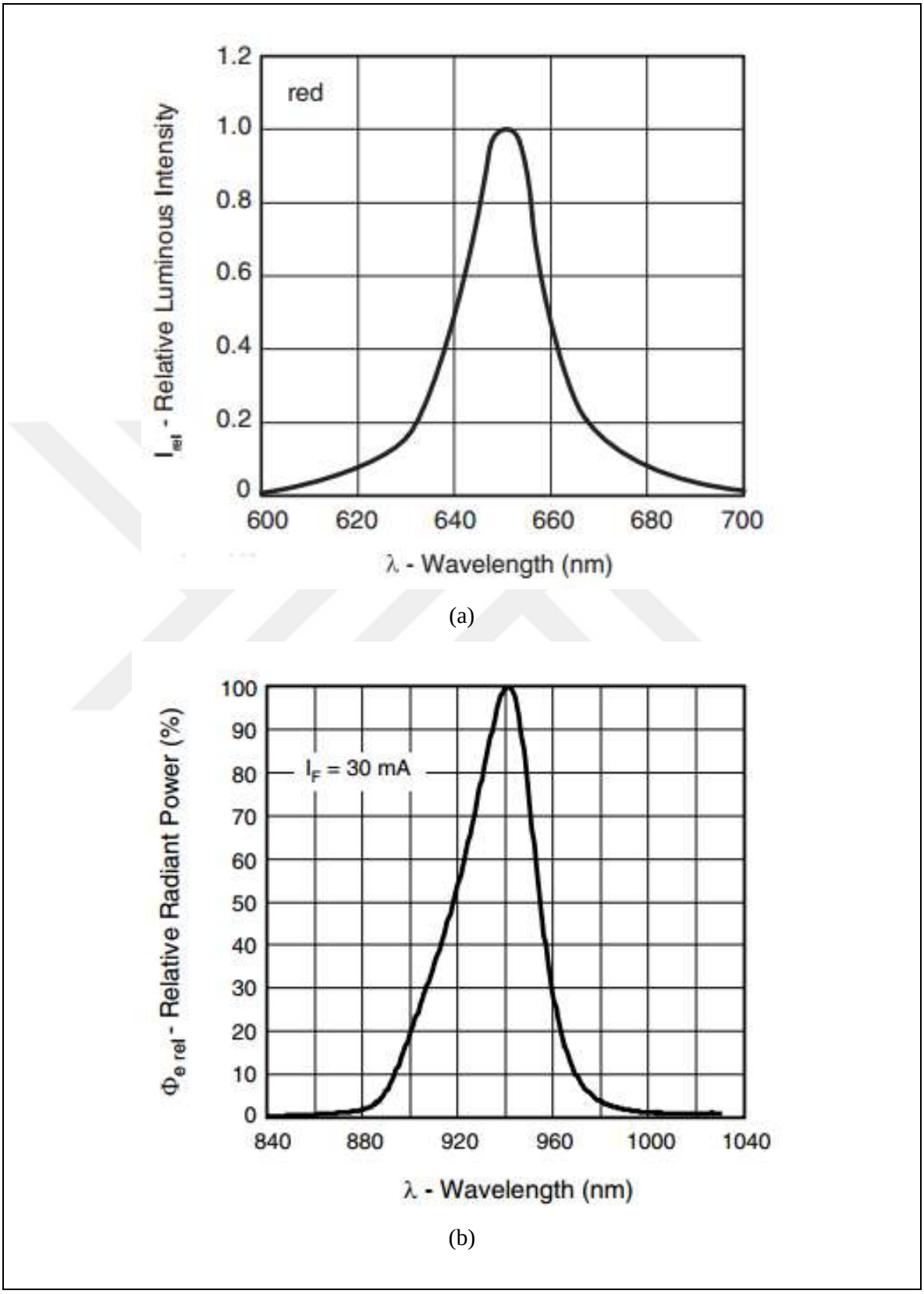

Figure 2.3. Relative intensity vs. wavelength for a) red LED and b) infra-red LED [52]

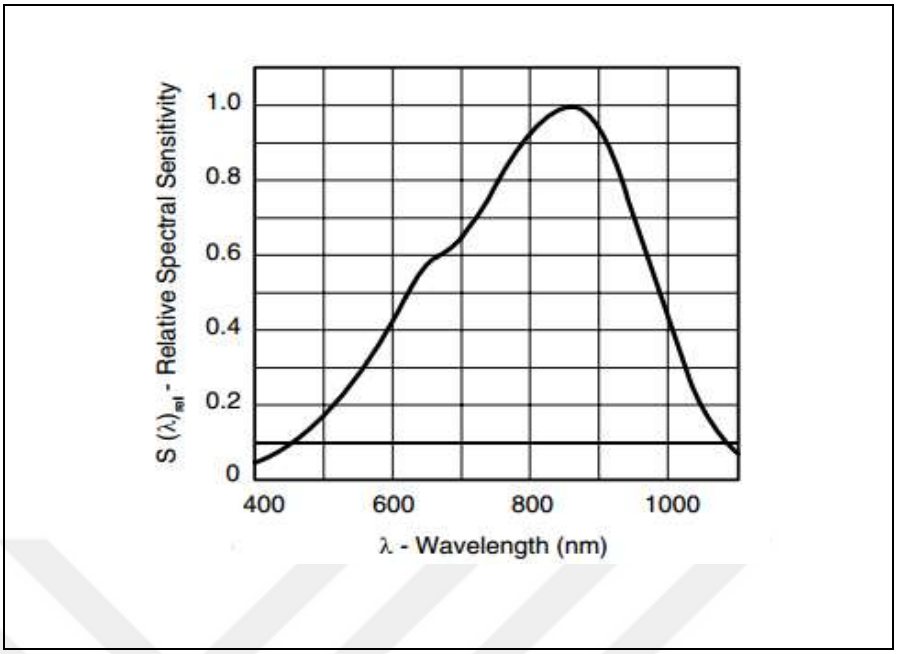

Figure 2.4. Relative Spectral Sensitivity vs. wavelength for BPW77NB phototransistor [53]

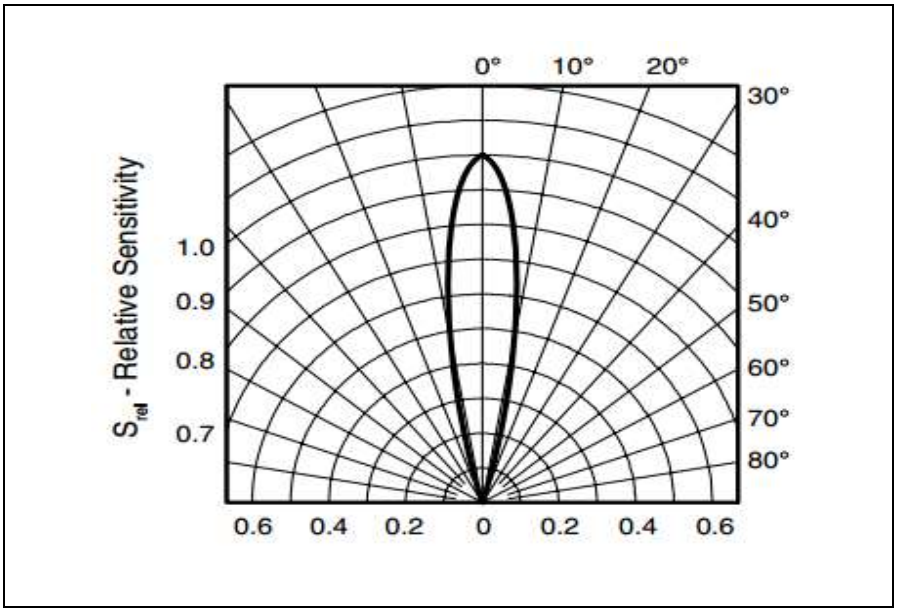

Figure 2.5. Relative radiant sensitivity vs. angular displacement for BPW77NB phototransistor [53].

Photoplethysmogram signals captured by phototransistors are noisy and therefore filtered by band-pass filters. In this study, this is achieved by an active filter. Active filters have active electronic components providing certain advantages over passive filters. Mainly, while filtering the signal, an active filter can also amplify it [51].

The active band-pass filter, designed in this study, is a second order one with low cut-off frequency of 1.59Hz and high cut-off frequency of 3.12Hz. The total gain of the filter is set to 10^4. The filter consist of a pair of LM358N operational amplifier. This amplifier is low power dual-operational amplifier with 1MHz operating frequency and 0.3V/μs slew rate and has wide power supply range between 1.5V and 16V [54]. In the current implementation, the op-amp is fed by +5Vdc supply voltage and consumes 0.6mA current while operating.

2.2. DATA ACQUISITION AND TRANSFER CARD

The sensor developed is controlled and Photoplethysmogram signals are acquired and transferred to a personal computer by Texas Instruments LAUNCHXL-RM42 (Texas Inc.)(see Figure 2.6) [55]. This launch pad provides an inexpensive development card and is equipped with 12-bit analog to digital converter modules, 45 general purposes I/O pins, serial communication interfaces and Hercules RM42L432 microcontroller, a dual core lock-step ARM Cortex-R4 based microcontroller unit that runs on 100MHz clock.

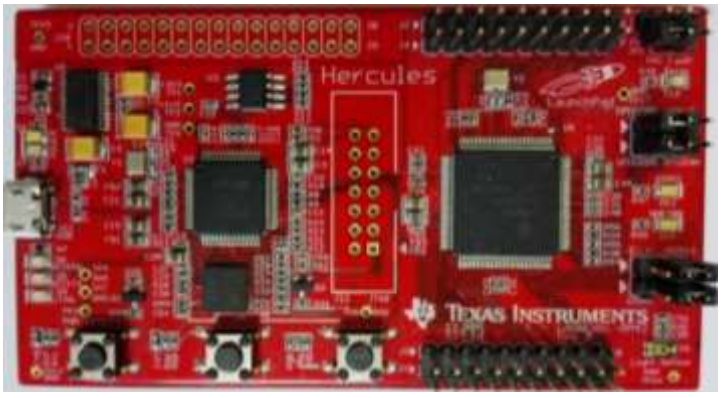

Figure 2.6. Texas Instruments LAUNCHXL-RM42

To make Hercules RM42L432 microcontroller functional, during this study, a microcontroller software was developed using Code Composer Studio 6.0.1 (Texas Instruments) and C programming language and loaded into the microcontroller. The flowchart of the software developed is as seen in Figure 2.7.

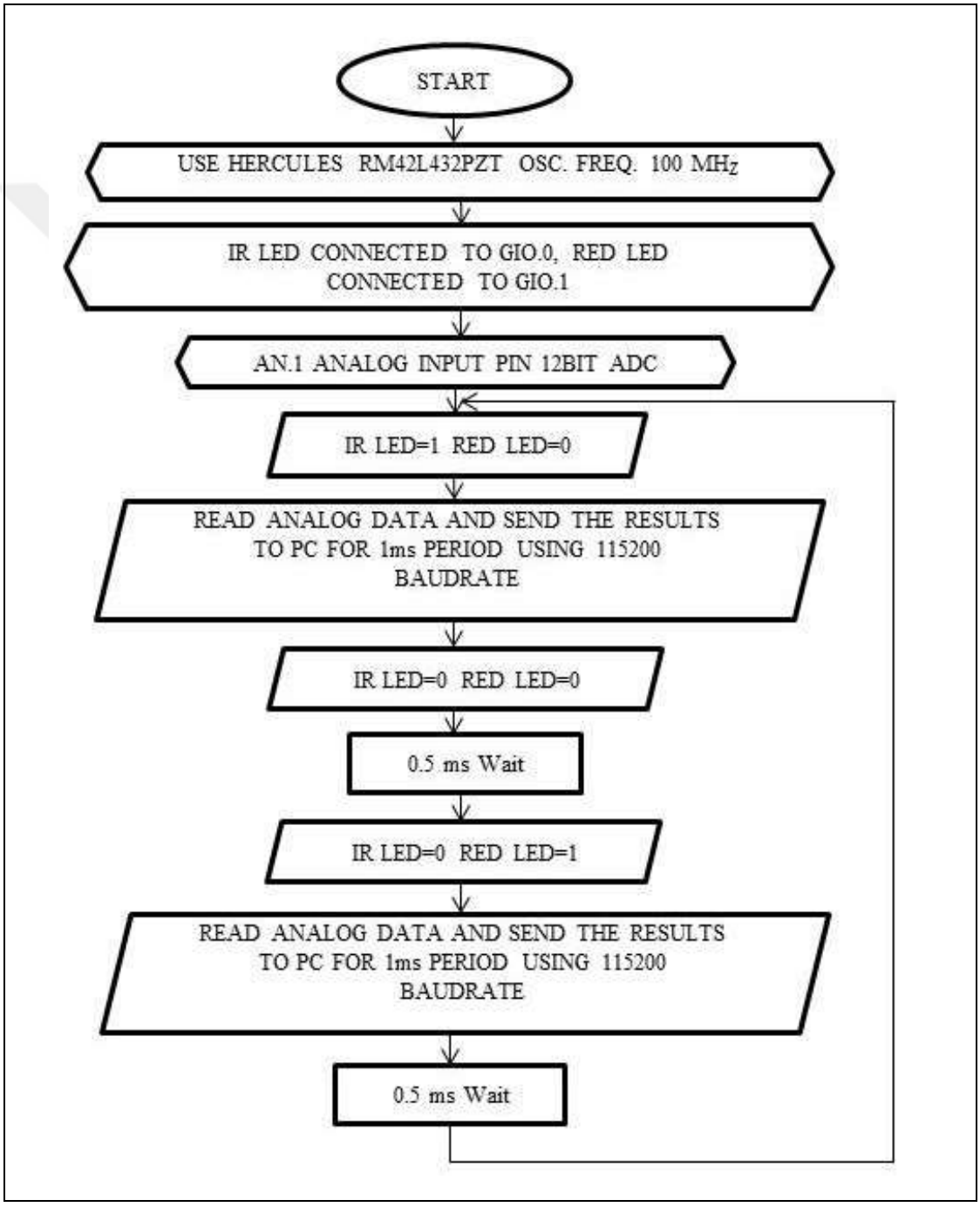

Figure 2.7. Flowchart of the microcontroller software developed

LED intensities controlled using data acquisition and transfer card (Texas Instrument LAUNCHXL-RM42). Figure 2.7 shows LED timings and sampling. Data transferring was also achieved using the data acquisition and transfer card using serial communication. Before serial communication data was digitalized (12-Bit resolution) using analog to digital conversion module of the data transfer card. Sample rate of the analog to digital conversion is 200 Hz. There is no parity bit and baud of the data transfer is 115200.

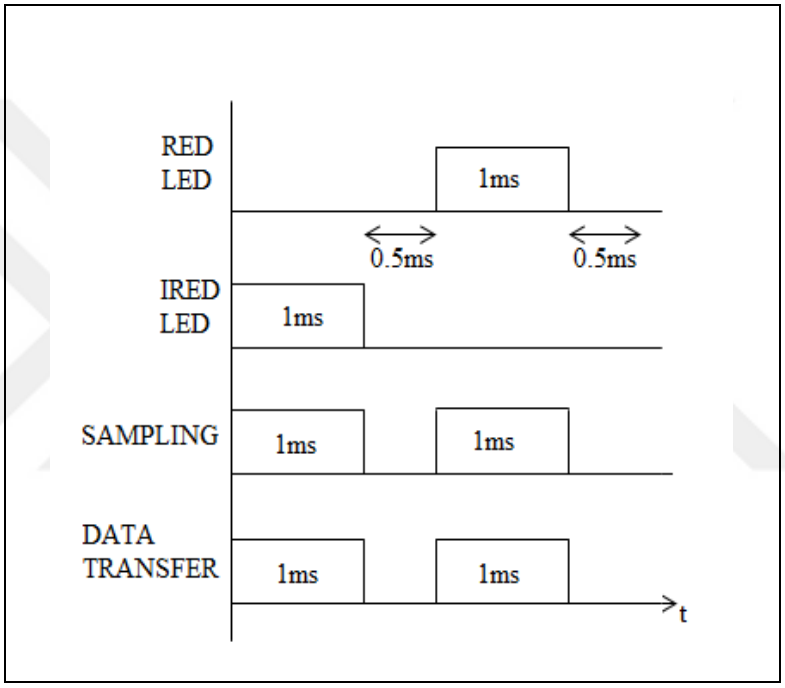

Figure 2.8. Timings for LEDs and sampling

2.3. DIGITAL FILTERING AND SPO_2 ESTIMATION

The signals transferred to computer till have artifacts and need some digital filtering. Photoplethysmogram signals are non-stationary signals. Therefore, instead of filtering the whole signal at once, it is preferable to use a moving window and then perform sub-filtering on the signal.

In digital filtering, windows are used for spectral harmonic analysis to reduce undesired effect of spectral leakage and have impact on many attributes of a harmonic processor including detectability, resolution, dynamic range, confidence and ease of implementation [56]. In this study, Hamming, Blackman, Bartlett, DPSS, Kaiser and Parzen-Rosenblatt windows are tested on the Photoplethysmogram signals captured by the device developed to accurately estimate oxygen saturation in the blood. These filters are updated to have the same window width of 50 and numerically implemented using MATLAB 2013b (Mathwork Inc. Natick, MA).

2.3.1. Hamming Window

This window is summation of the shifted Dirichlet kernel with optimized minimum and maximum side lobes defined using [57].

$$w(n) = 0.54 - 0.46\cos\left(\frac{2\pi n}{N-1}\right) \tag{2.1}$$

Here N is the size of the window. Relative side-lobe attenuation is -42.3 dB, main-lobe width (-3 dB) is 0.051 and leakage factor is 0.04% for the Blackman[57]. Plots of this window in time and frequency domains are as seen in Figure 2.9.

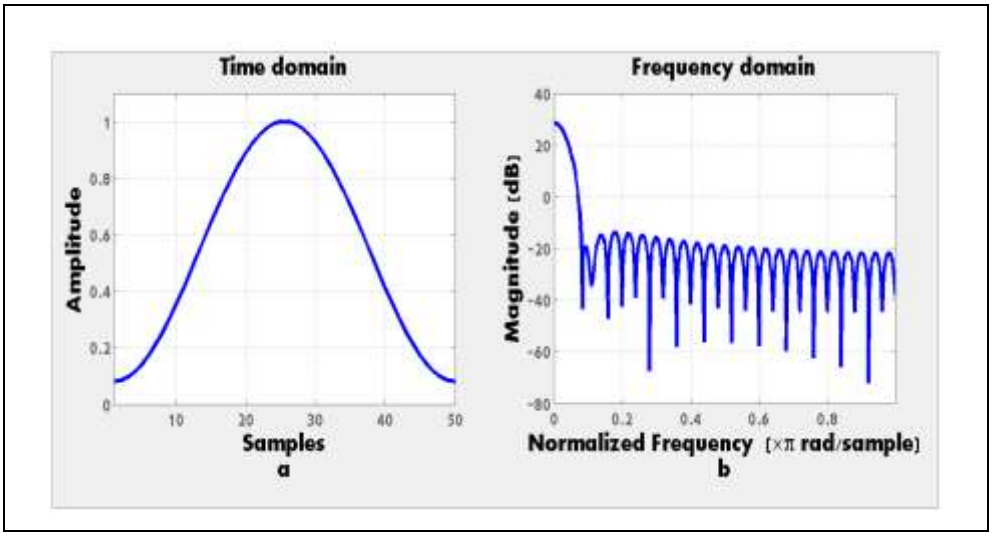

Figure 2.9. Plot of Hamming window in a) time domain and in b) frequency domain

2.3.2. Blackman Window

This window is constructed with any K nonzero coefficients and achieve a (2K-1) summation of kernels. If K value is small integer, main lobe will be narrow. Blackman examined the window for K=3 and found the value of the nonzero coefficients which place in 3.5 Hz and 4.5 Hz [68]. Relative side-lobe attenuation is -58.1 dB, main-lobe width (-3 dB) is 0.066 and leakage factor is 0% for the Blackman window. Equation (4.2) shows Blackman window;

$$w(n) = a_0 - a_1 \cos\left(\frac{2\pi n}{N-1}\right) + a_2 \left(\frac{4\pi n}{N-1}\right) \tag{2.2}$$

In this study, the coefficients a_0, a_1 and a_2 are set to 0.42, 0.50 and 0.08, respectively. Plots of this window in time and frequency domains are as seen in Figure 2.10.

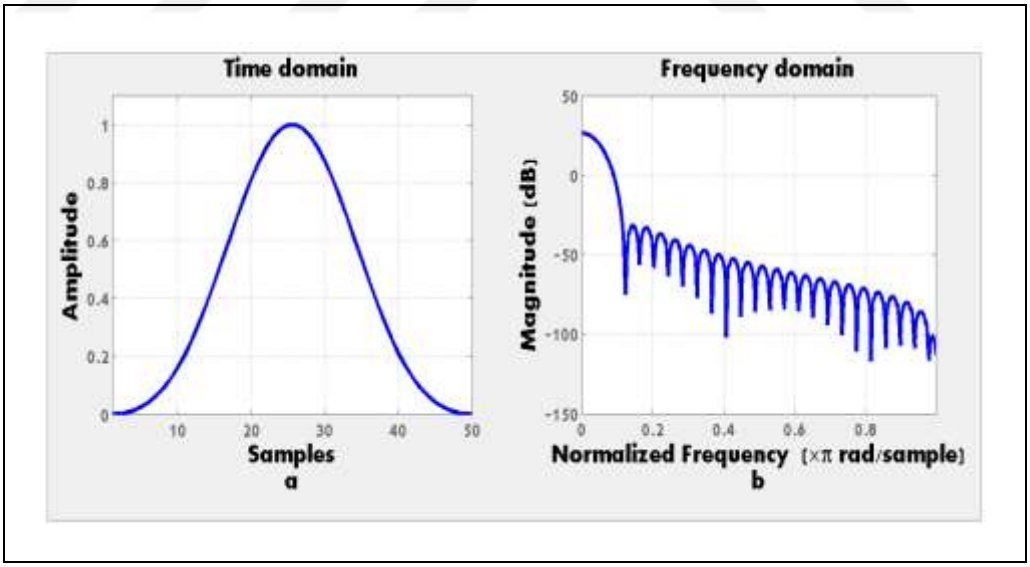

Figure 2.10. Plot of Blackman window in a) time domain and in b) frequency domain

2.3.3. Bartlett Window

This window is a triangular window as a result of convolution of two (*N*-1)/2 rectangular windows, with a main lobe twice as wide as that of a rectangular window of length *N*, and described using [59]. Relative side-lobe attenuation is -26.5 dB, main-lobe width (-3 dB) is 0.051 and leakage factor is 0.28% for the Bartlett window.

$$w(n) = a_0 - a_1 > \left|\frac{n}{N-1} - \frac{1}{2}\right| - a_2 \cos\left(\frac{2\pi n}{N-1}\right) \tag{2.3}$$

In this study, the coefficients a_0, a_1 and a_2 are set to 0.62, 0.48 and 0.38, respectively. Plots of this window in time and frequency domains are as seen in Figure 2.11.

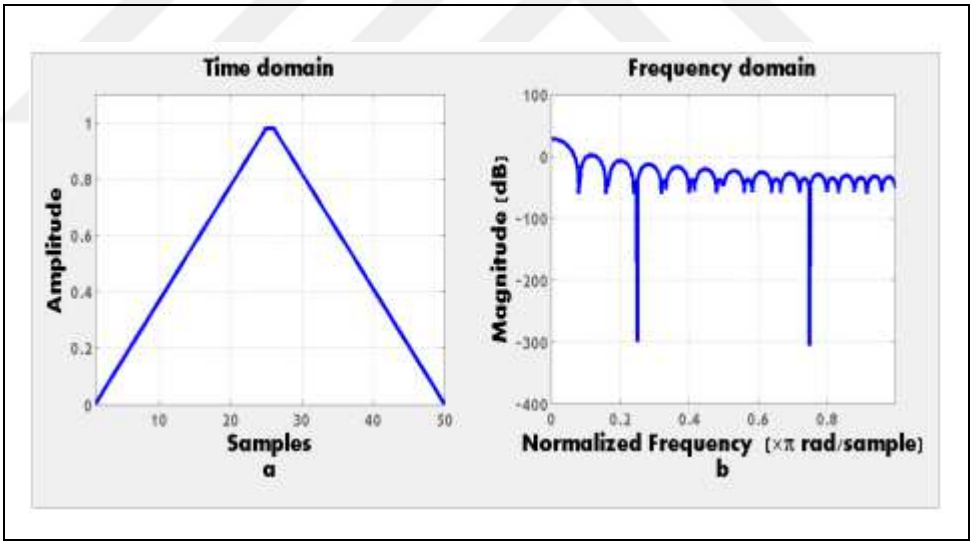

Figure 2.11. Plot of Bartlett window in a) time domain and in b) frequency domain

2.3.4. Digital Prolate Spheroidal Sequence (DPSS) Window

This window has the maximal energy concentration in the main lobe and consists of an Eigen vector corresponding to the largest Eigen value of the integration equation by [60].

Relative side-lobe attenuation is -124 dB, main-lobe width (-3 dB) is 0.082 and leakage factor is 0% for DPSS window.

$$\int_{-\omega_c}^{\omega_c} W(v)\frac{\sin\left(\pi D(\omega - v)\right)}{\pi(\omega - v)}\, d\omega = \lambda W(\omega) \tag{2.4}$$

here W(ω) is continuous function of $\omega \in (-\infty,\infty)$, the function of W($\omega$) maximize the main lobe energy and total energy ratio. Main lobe bandwidth is $2\omega_c$. Plots of this window in time and frequency domains are as seen in Figure 2.12.

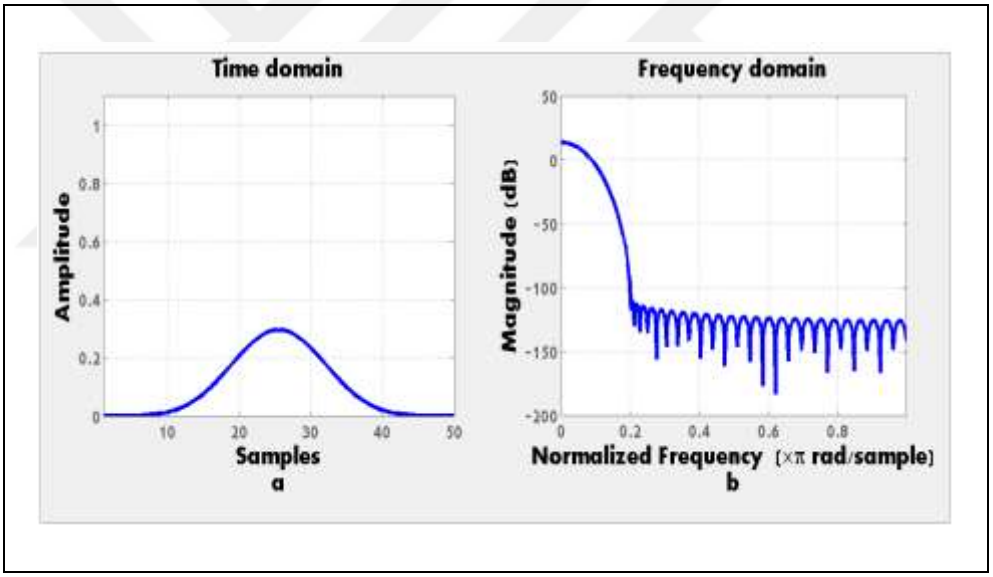

Figure 2.12. Plot of DPSS window in a) time domain and in b) frequency domain

2.3.5. Kaiser Window

This window is one parameter window inherited from Bessel function and defined by [61]

$$w(n) = \begin{cases} \dfrac{I_0\left(\beta\sqrt{1-\left(\frac{n}{N/2}\right)^2}\right)}{I_0(\beta)}, -\dfrac{N-1}{2} < 0 < \dfrac{N-1}{2} \\ 0 \quad , \ elsewhere \end{cases} \tag{2.5}$$

here β provides a continuity over the fundamental window trade-off between side-lobe and main-lobe width. Larger β values produce lower side-lobe level and wider main-lobe but wide main reduces the frequency resolution. I_0 is the zero-ordered modified Bessel function of the first kind given by

$$I_0(x) = \sum_{k=0}^{\infty}\left[\frac{(x/2)^k}{k!}\right]^2 \tag{2.6}$$

This window reduces the rectangular window for β =0. Asymptotic roll-off is 6 dB/octave. Relative side-lobe attenuation is -119.8 dB, main-lobe width (-3 dB) is 0.086 and leakage factor is 0% for Kaiser window. Sometimes, Kaiser window is parameterized by α parameter where $\beta=\pi\alpha$. Plots of this window in time and frequency domains are as seen in Figure 2.13.

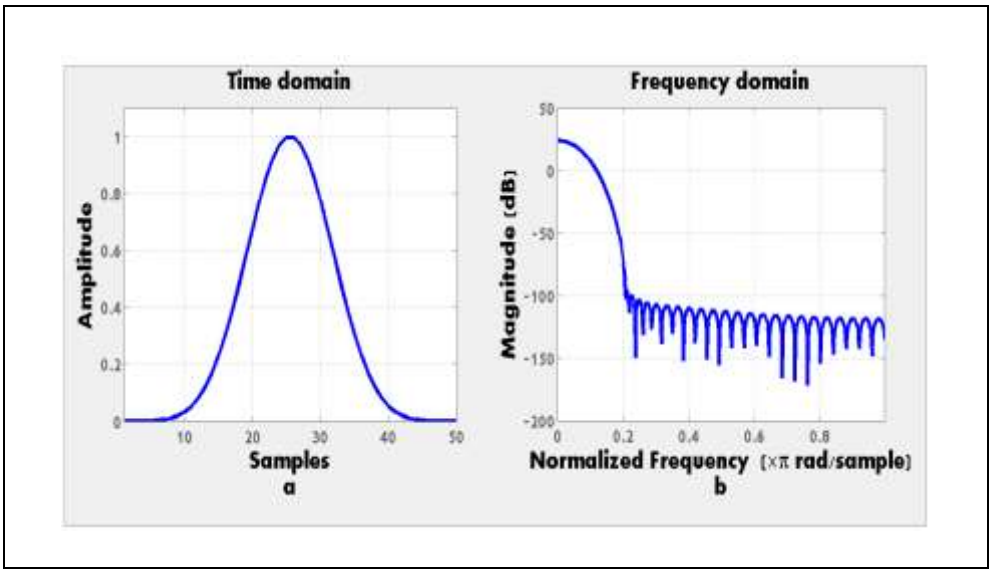

Figure 2.13. Plot of Kaiser window in a) time domain and in b) frequency domain

2.3.6. Parzen-Roseblatt Window

It is termed Kernel Density Estimation. This method uses neighboring observation of a point *x* for estimation [62].

$$\hat{f}_h(x) = \frac{1}{Nh}\sum_{i=1}^{N} K\left(\frac{x - x_i}{h}\right) \tag{2.7}$$

K(•) is a kernel function that has zero mean. *h* is smoothing parameter determining the width of the window. Plot of this window in time domain and frequency domain as seen in figure 2.14. Relative side-lobe attenuation is -53 dB, main-lobe width (-3 dB) is 0.070 and leakage factor is 0%.

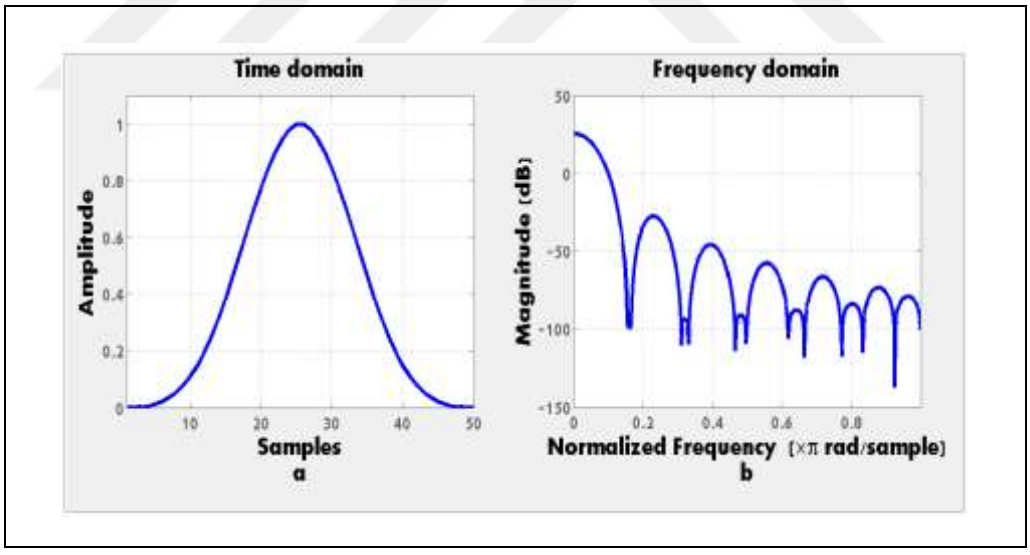

Figure 2.14. Plot of Parzen-Rosenblatt window in a) time domain and in b) frequency domain

2.3.7. SPO2 Estimation

To estimate SPO_2 percentages, the device developed in this study is calibrated with a non-invasive calibration method with the use of a periodically calibrated Rossmax SA210 pulse oximeter (Rossmax Inc.) sited at Yeditepe University Hospital. (Consent of Yeditepe University Hospital administration was secured).

Rossmax SA210 pulse oximeter, seen in Figure 2.15, is a well-known handheld pulse oximeter to measure oxygen saturation in blood and pulse rate from adults over 40kgs at hospitals. It has a transmissive sensor equipped with a dual light source from a red LED and an infrared red LED. The wavelength of the red LED and infrared LED is 660nm and 905/880nm, respectively with maximum optical output power of 4mW. The oximeter performs measurements with very low mean error (~2%) between 70-100% values.

Figure 2.15. Rossmax SA210 pulse oximeter [63]

Eight healthy male volunteers aging between 25-35 years were enrolled in calibration study after giving consent. Prior to examinations, all volunteers took a rest for five minutes. From the right index finger of all volunteers, a set of SpO_2 estimates are directly obtained using the calibrated device and a set of RR estimates are also determined for the same body location using the device developed in this study. Linear regression analysis based on least mean square method is performed to get a "transformation" equation between RR estimates and "reference" SpO_2 estimates. The mean difference between the "reference" SpO_2 estimates from the calibrated device and the SpO_2 estimates computed from the RR estimates given by the device developed is calculated as the mean calibration error using [64].

$$e_{calibration} = \frac{1}{n}\sum_{i=1}^{n}|\hat{y}_i - y_i| \tag{2.8}$$

here n is total measurement number for each volunteer. $\hat{y}_i$ is the reference SpO_2 measured and y_i is the SpO_2 estimated for the i-th volunteer. This mean error is subtracted from each SpO_2 estimate and the resultant values are considered as the calibrated SpO_2 estimates from the device developed. Calibrated SpO_2 and previously determined RR estimates by the device are next input to linear regression analysis. The analysis outputs two parameters: a slope coefficient and a bias. The calibration procedure explained above was performed for each window given in the materials and methods section and the values of the parameters are recorded for future use.

Twenty-one volunteers (10 male, 11 female and mean age 23) were used to test the pulse oximeter device. Prior to examinations, all volunteers took a rest for five minutes. Using the "transformation" equation obtained, SpO_2 estimations were performed for RR estimates determined by the device developed from the right index fingertip and from the intercostal artery in the center of the left chest, respectively.

2.4. STATISTICAL ANALYSIS

Systematic differences between SpO_2 estimates by the device developed from the right index fingertip and the left chest center were tested using independent samples t-test either a pooled or as separate variance as determined by the Levene's test for equality of

variances. A *P* value <0.5 was considered to be statistically significant. All statistical analysis were performed by using Microsoft Excel 2010 (Microsoft, USA).

3. RESULTS

Figure 3.1. shows raw Photoplethysmogram signals acquired using the device developed from the fingertip and the chest, respectively. Digital filtering based on Hamming window, Blackman window, Bartlett window, DPSS window, Kaiser window and Parzen-Rosenblatt window was applied to the signals to eliminate noise. Blue and red lines represent infra-red and red data for all figures.

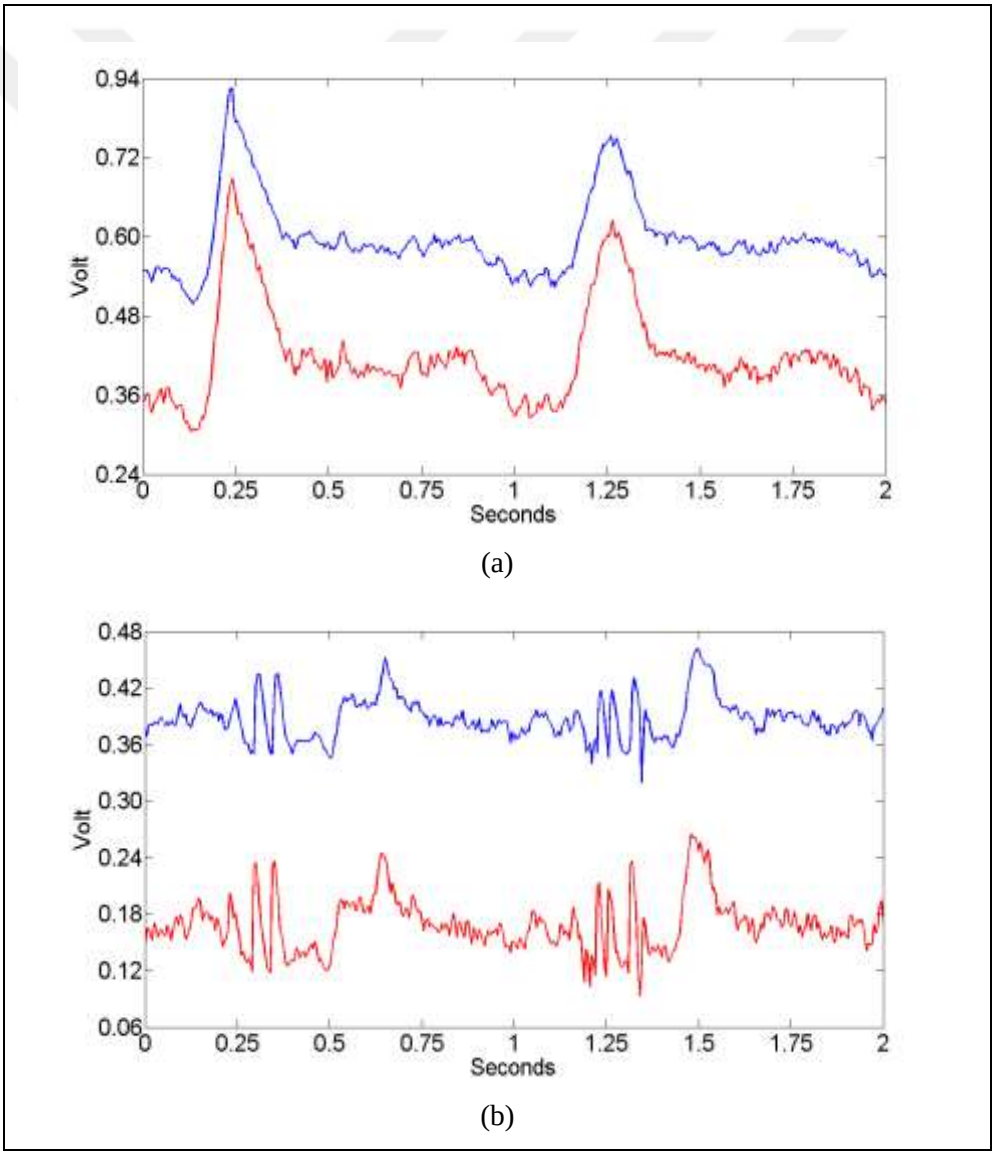

Figure 3.1. Raw Photoplethysmograms recorded from a) right index fingertip b) chest

The outputs of the digital filtering with Hamming window are as seen in Figures 3.2

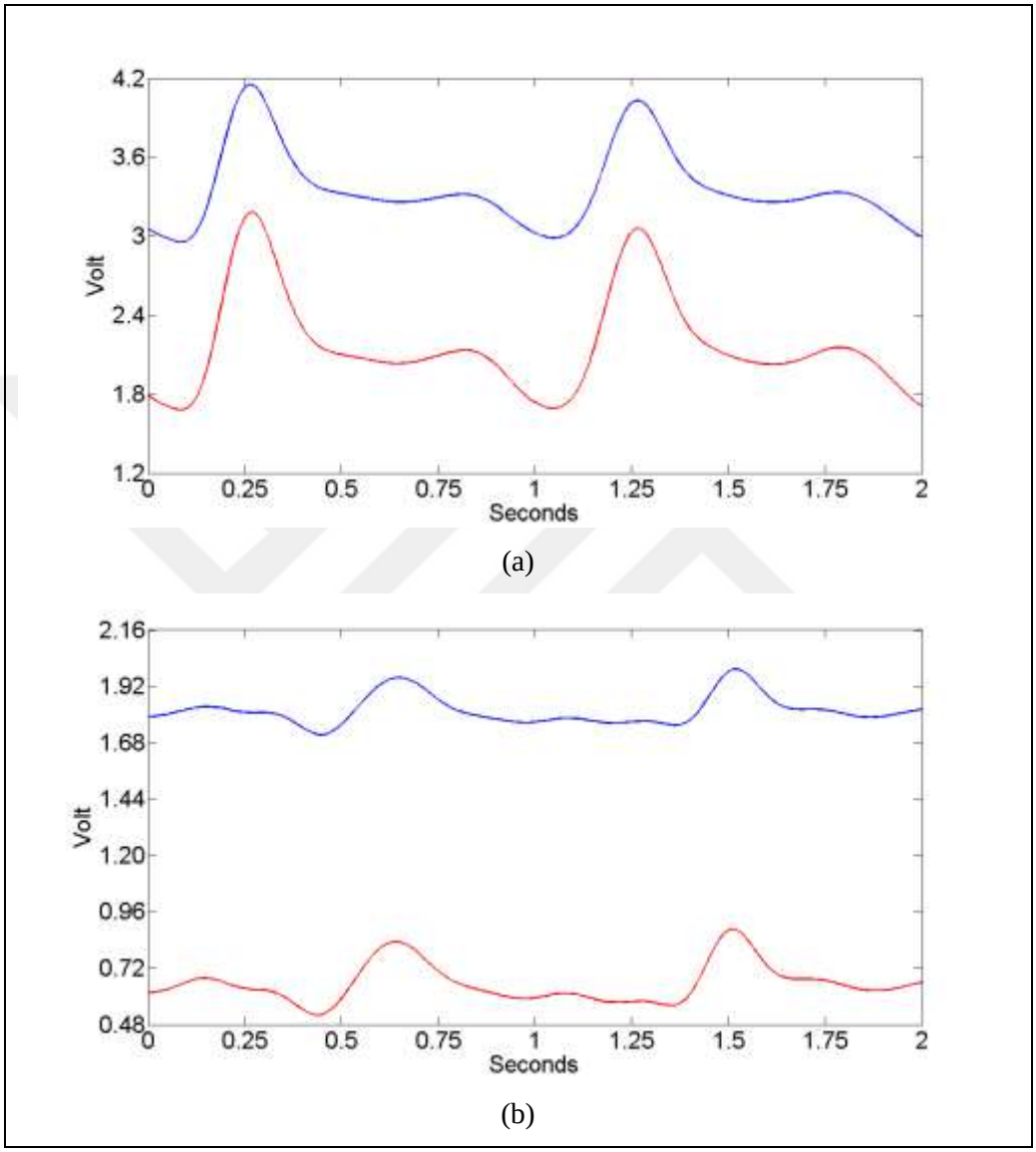

Figure 3.2. Filtered signals from a) fingertip b) chest by using Hamming window.

Table 3.1 shows the SpO_2 measurement results from the calibrated device and RR values estimated by the pulse oximeter developed in this project. The plot for those values are as seen in Figure 3.3. They are used to get the SpO_2 equation (Equitation 3.1) for Hamming window. The difference between the measurements and estimations lead to a mean error of 4.58.

Table 3.1. SpO_2 estimations from fingertip using Hamming window

Volunteer	Measured SpO_2	RR-Hamming	Estimated SpO_2	Error
#1	96	0.61	101.67	5.67
#2	97	0.58	101.67	4.67
#3	96	0.68	97.43	1.43
#4	98	0.56	102.64	4.64
#5	96	0.64	99.38	3.38
#6	96	0.53	104.00	8.00
#7	97	0.66	98.58	1.58
#8	97	0.52	104.26	7.26
			Total Error	36.62
			Mean Error	4.58

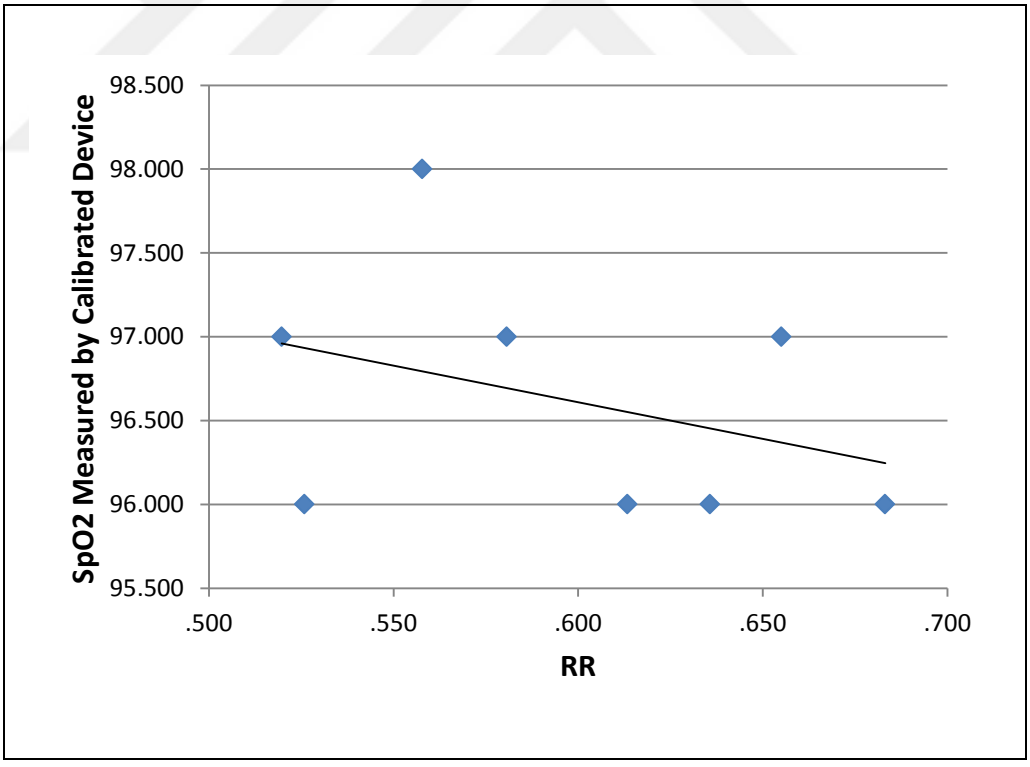

Figure 3.3. Calibration of SpO_2 estimations for Hamming window

$$SpO_{2Hamming} = -4.37RR + 99.23 \quad (3.1)$$

The outputs of the digital filtering with Blackman windows are as seen in Figure 3.4.

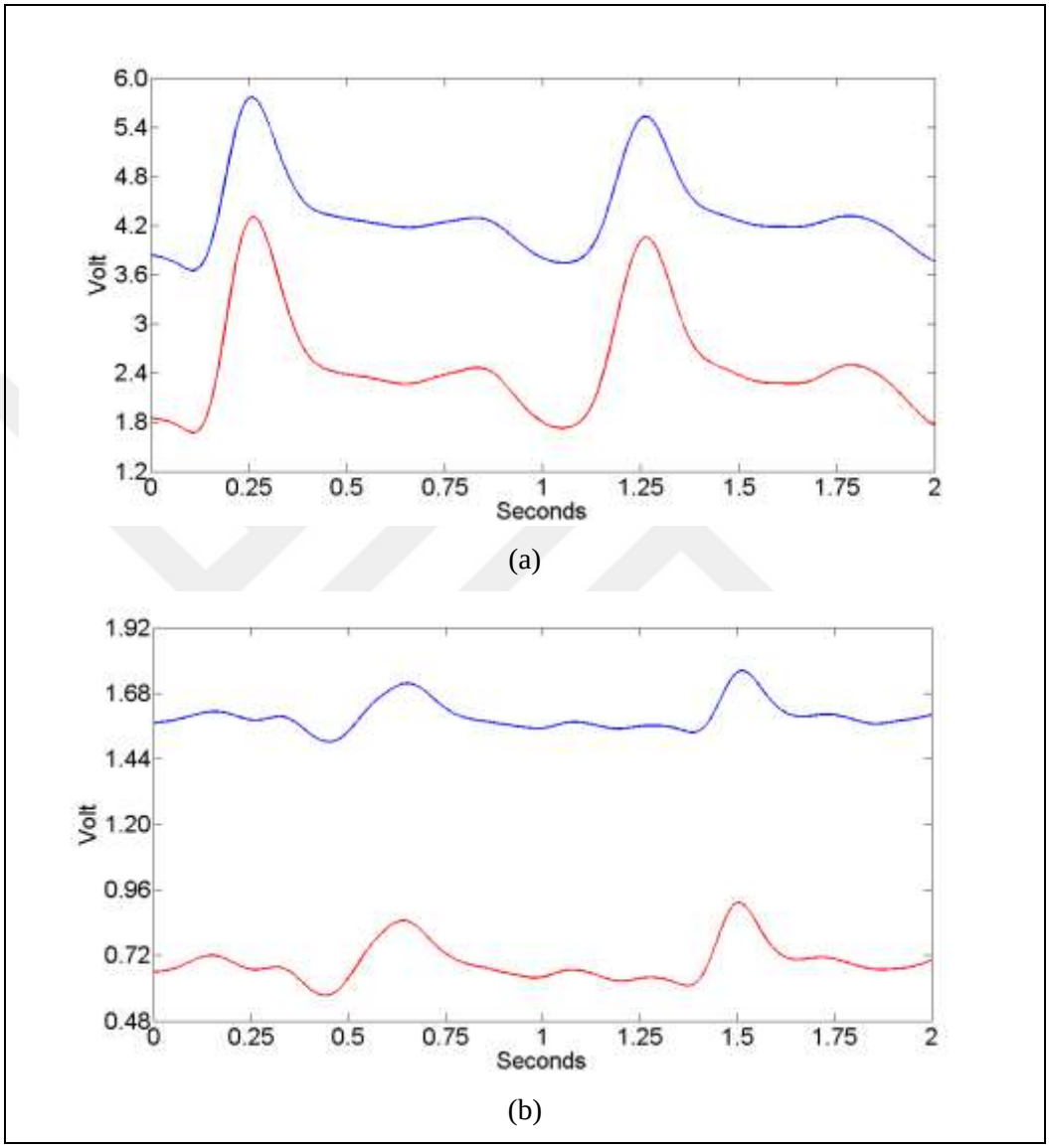

Figure 3.4. Filtered signals from a) fingertip b) chest by using Blackman window.

Table 3.2 shows the SpO_2 measurement results from the calibrated device and RR values estimated by the pulse oximeter developed. The plot for those values are as seen in Figure 3.5. They are used to get the SpO_2 equation (Equitation 3.2) for Blackman window. The difference between the measurements and estimations lead to a mean error of 5.05.

Table 3.2. SpO_2 estimations from fingertip using Blackman window

Volunteers	Measured SpO_2	RR-Blackman	Estimated SpO2	Error
#1	96	0.59	101.14	5.14
#2	97	0.56	102.57	5.57
#3	96	0.67	97.87	1.87
#4	98	0.55	103.15	5.15
#5	96	0.63	99.56	2.56
#6	96	0.51	104.89	8.89
#7	97	0.64	99.03	2.03
#8	97	0.50	105.22	8.22
			Total Error	40.44
			Mean Error	5.05

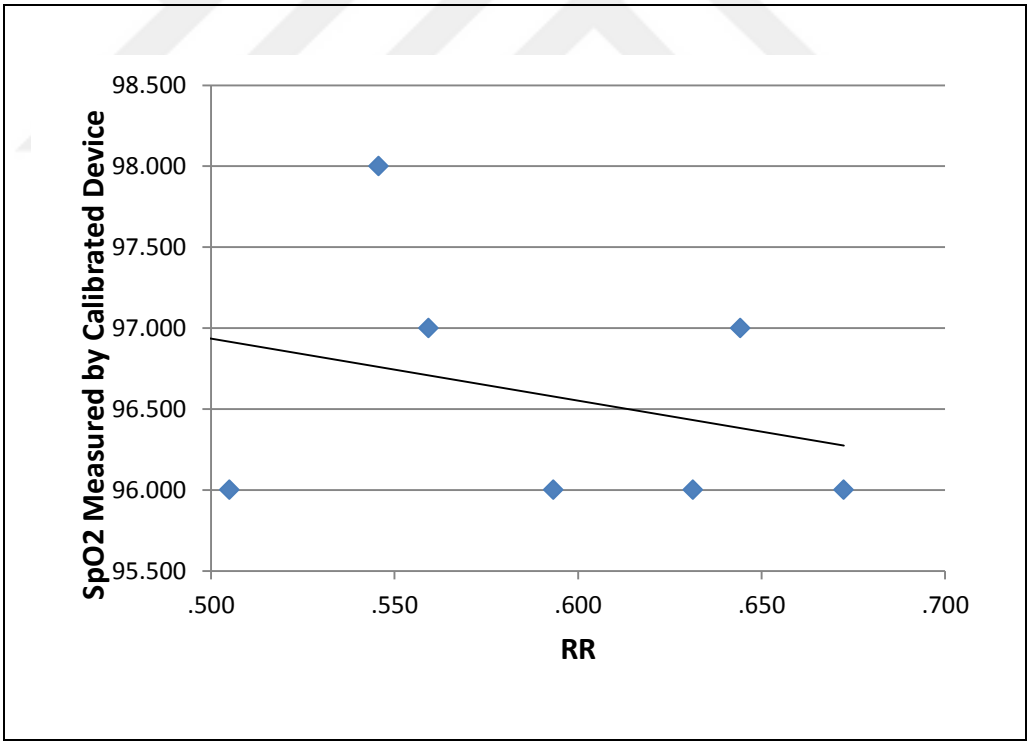

Figure 3.5. Calibration of SpO_2 estimations for Blackman window.

$$SpO_{2Blackman} = -3.83RR + 98.85 \quad (3.2)$$

The outputs of the digital filtering with Bartlett windows are as seen in Figure 3.6.

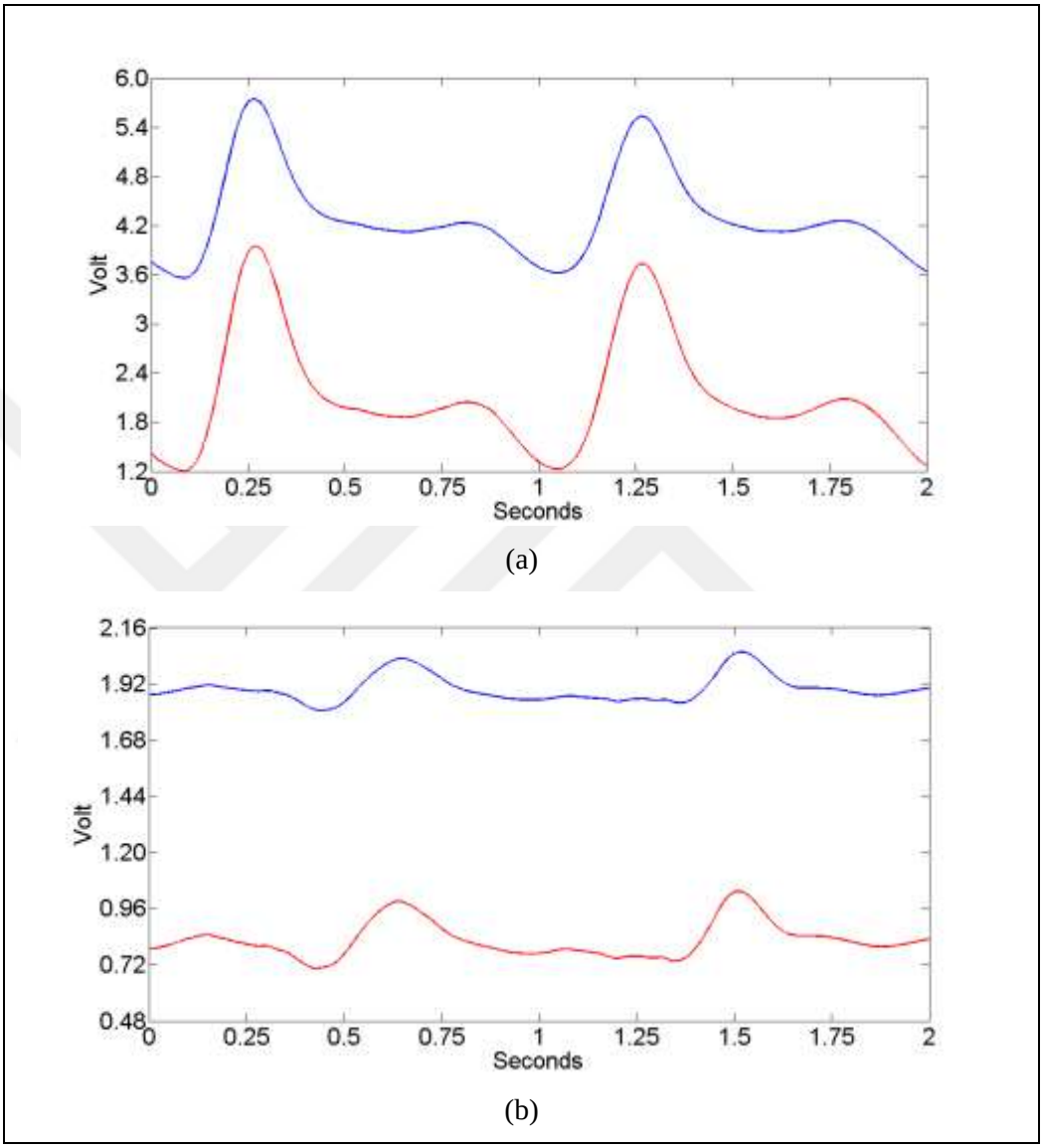

Figure 3.6. Filtered signals from a) fingertip b) chest by using Bartlett window.

Table 3.3 shows the SpO_2 measurement results from the calibrated device and RR values estimated by the pulse oximeter developed in this project. The plot for those values are as seen in Figure 3.7. They are used to get the SpO_2 equation (Equitation 3.3) for Bartlett window. The difference between the measurements and estimations lead to a mean error of 4.36.

Table 3.3. SpO_2 estimations from fingertip using Bartlett window

Volunteers	Measured SpO_2	RR-Bartlett	Estimated SpO2	Error
#1	96	0.61	100.24	4.24
#2	97	0.58	101.61	4.61
#3	96	0.68	97.38	1.38
#4	98	0.56	102.60	6.60
#5	96	0.64	99.36	3.36
#6	96	0.53	103.93	7.93
#7	97	0.66	98.54	1.54
#8	97	0.52	104.20	7.20
			Total Error	34.85
			Mean Error	4.36

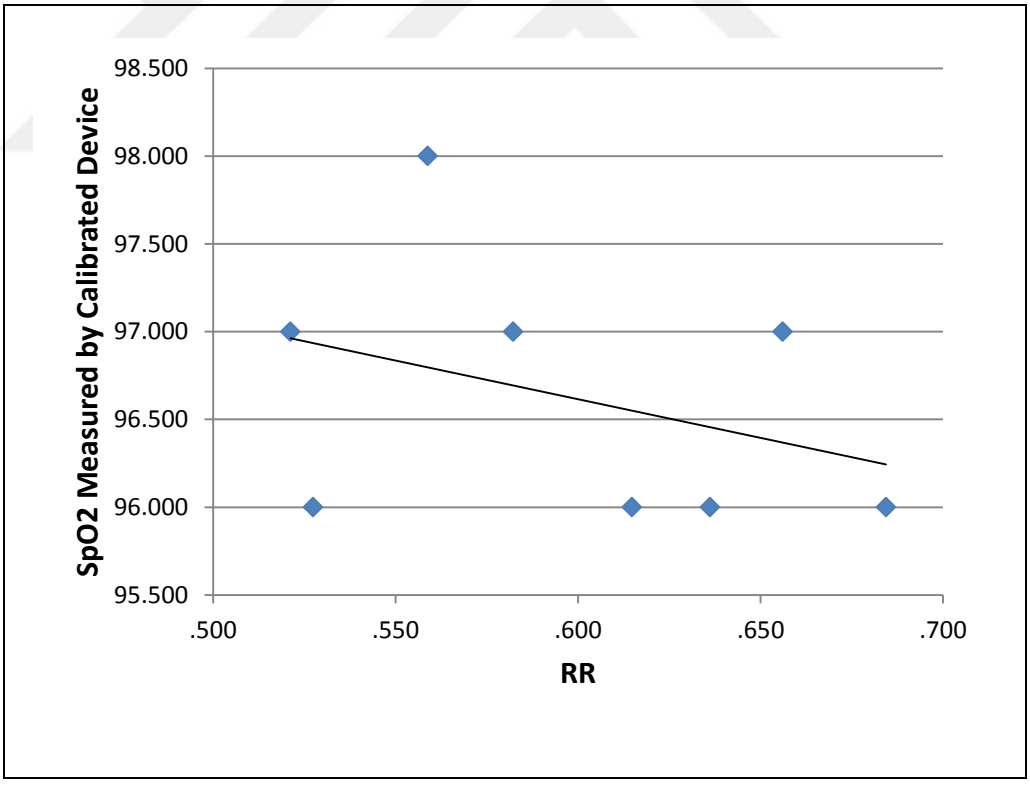

Figure 3.7. Calibration of SpO_2 estimations for Bartlett window.

$$SpO_{2Batlett} = -4.40RR + 99.25 \quad (3.3)$$

The outputs of the digital filtering with DPSS windows are as seen in Figure 3.8.

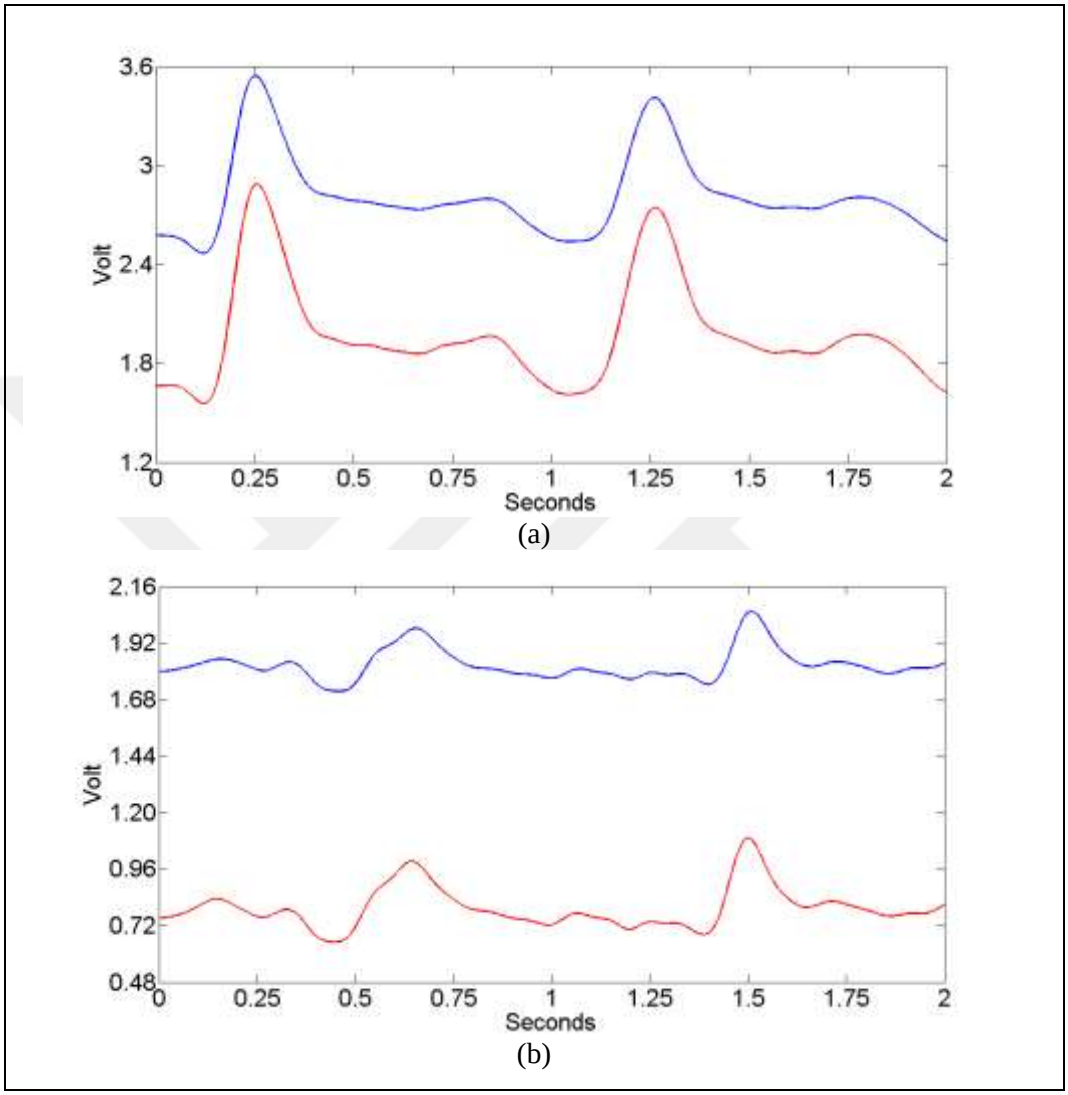

Figure 3.8. Filtered signals from a) fingertip b) chest by using DPSS window.

Table 3.4 shows the SpO_2 measurement results from the calibrated device and RR values estimated by the pulse oximeter developed in this project. The plot for those values are as seen in Figure 3.9. They are used to get the SpO_2 equation (Equitation 3.4) for DPSS window. The difference between the measurements and estimations lead to a mean error of 5.54.

Table 3.4. SpO_2 estimations from fingertip using DPSS window

Volunteers	Measured SpO_2	RR-DPSS	Estimated SpO2	Error
#1	96	0.58	101.86	5.86
#2	97	0.54	103.26	6.26
#3	96	0.67	98.17	2.17
#4	98	0.54	103.51	5.51
#5	96	0.63	99.66	3.66
#6	96	0.49	105.59	9.59
#7	97	0.64	99.32	2.32
#8	97	0.48	105.96	8.96
			Total Error	44.32
			Mean Error	5.54

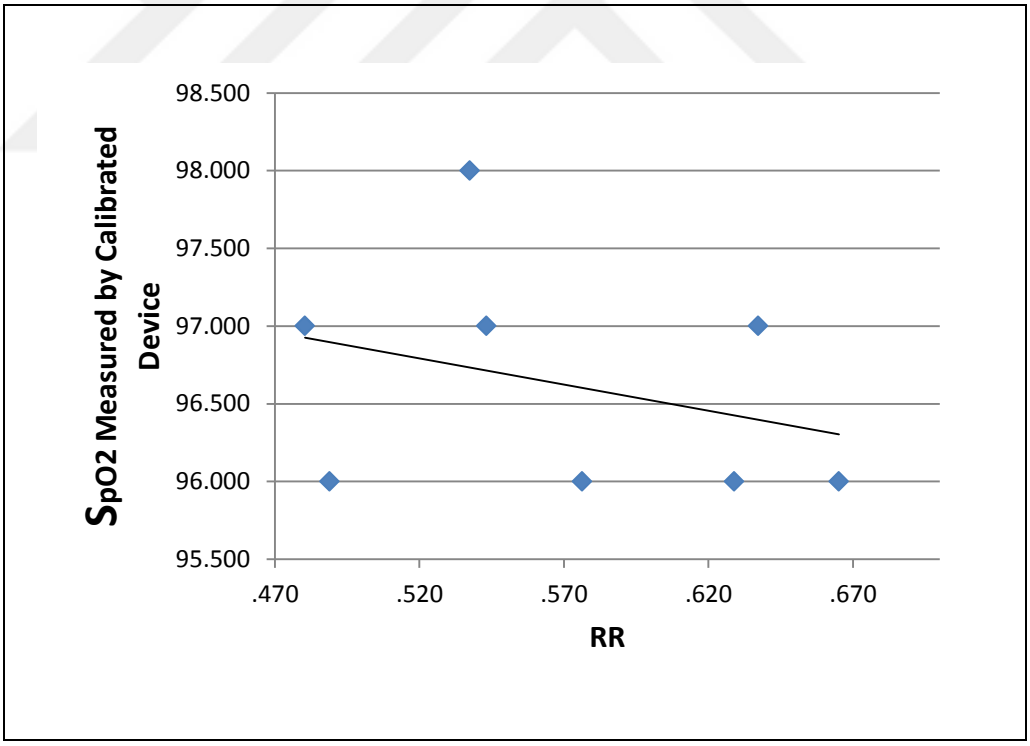

Figure 3.9. Calibration of SpO_2 estimations for DPSS window.

$$SpO_{2DPSS} = -3.37RR + 98.54 \quad (3.4)$$

The outputs of the digital filtering with Kaiser windows are as seen in Figure 3.10

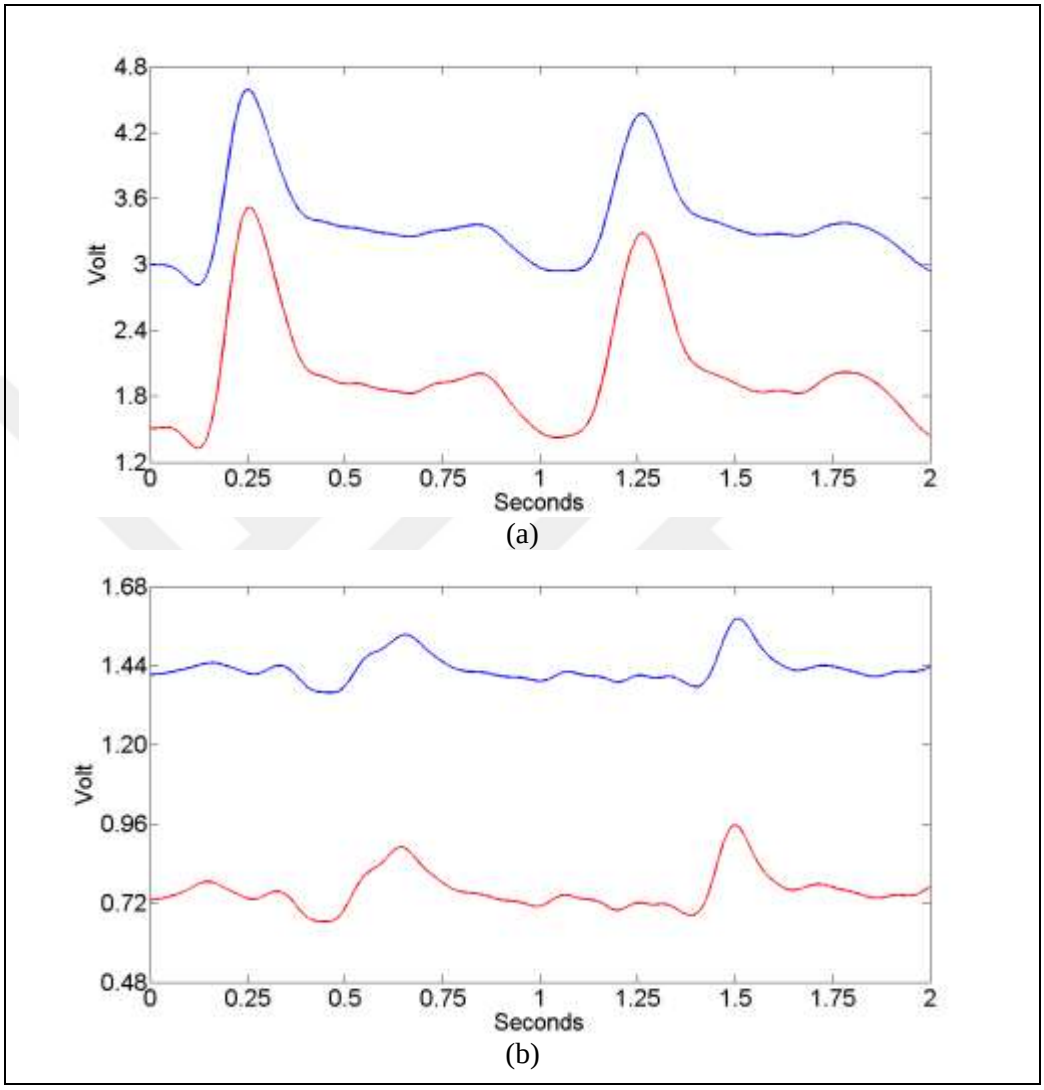

Figure 3.10. Filtered signals from a) fingertip b) chest by using Kaiser window.

Table 3.5 shows the SpO_2 measurement results from the calibrated device and RR values estimated by the pulse oximeter developed in this project. The plot for those values are as seen in Figure 3.11. They are used to get the SpO_2 equation (Equitation 3.5) for Kaiser window. The difference between the measurements and estimations lead to a mean error of 5.60.

Table 3.5. SpO_2 estimations from fingertip using Kaiser window

Volunteers	Measured SpO_2	RR-Kaiser	Estimated SpO2	Error
#1	96	0.57	101.95	5.95
#2	97	0.54	103.35	6.35
#3	96	0.66	98.20	2.20
#4	98	0.54	103.55	5.55
#5	96	0.63	99.67	3.67
#6	96	0.49	105.68	9.68
#7	97	0.64	99.35	2.35
#8	97	0.48	106.05	9.05
			Total Error	44.80
			Mean Error	5.60

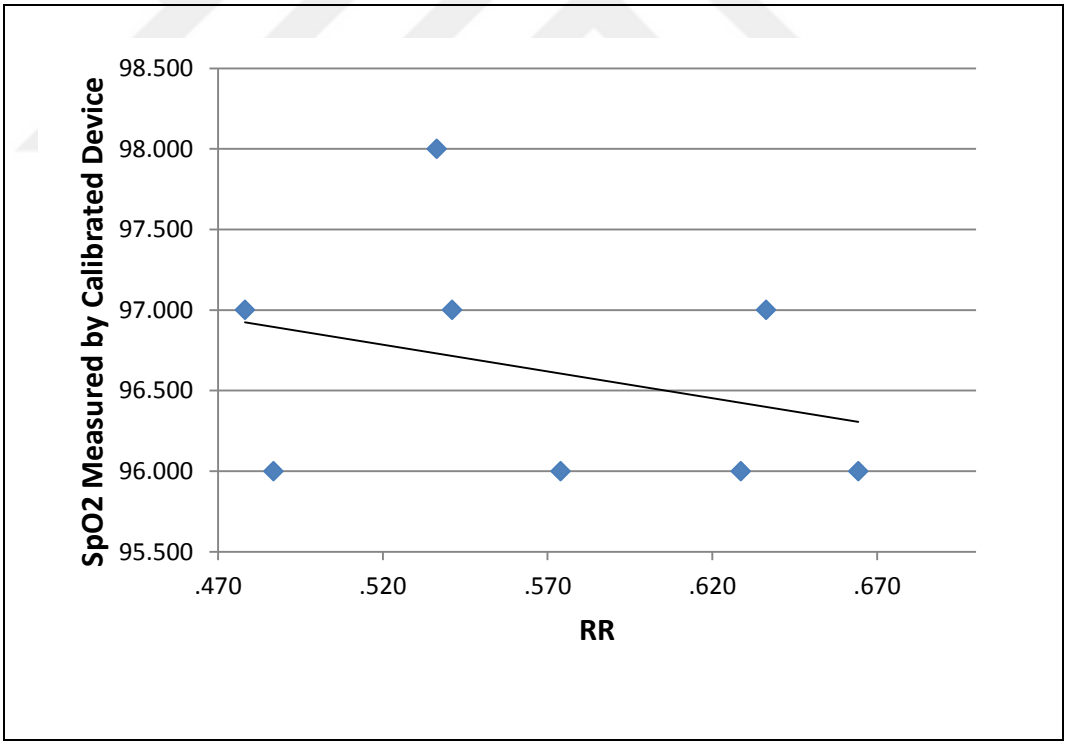

Figure 3.11. Calibration of SpO_2 estimations for Kaiser window.

$$SpO_{2Kaiser} = -3.31RR + 98.51 \quad (3.5)$$

The outputs of the digital filtering with Parzen-Rosenbaltt windows are as seen in Figure 3.12.

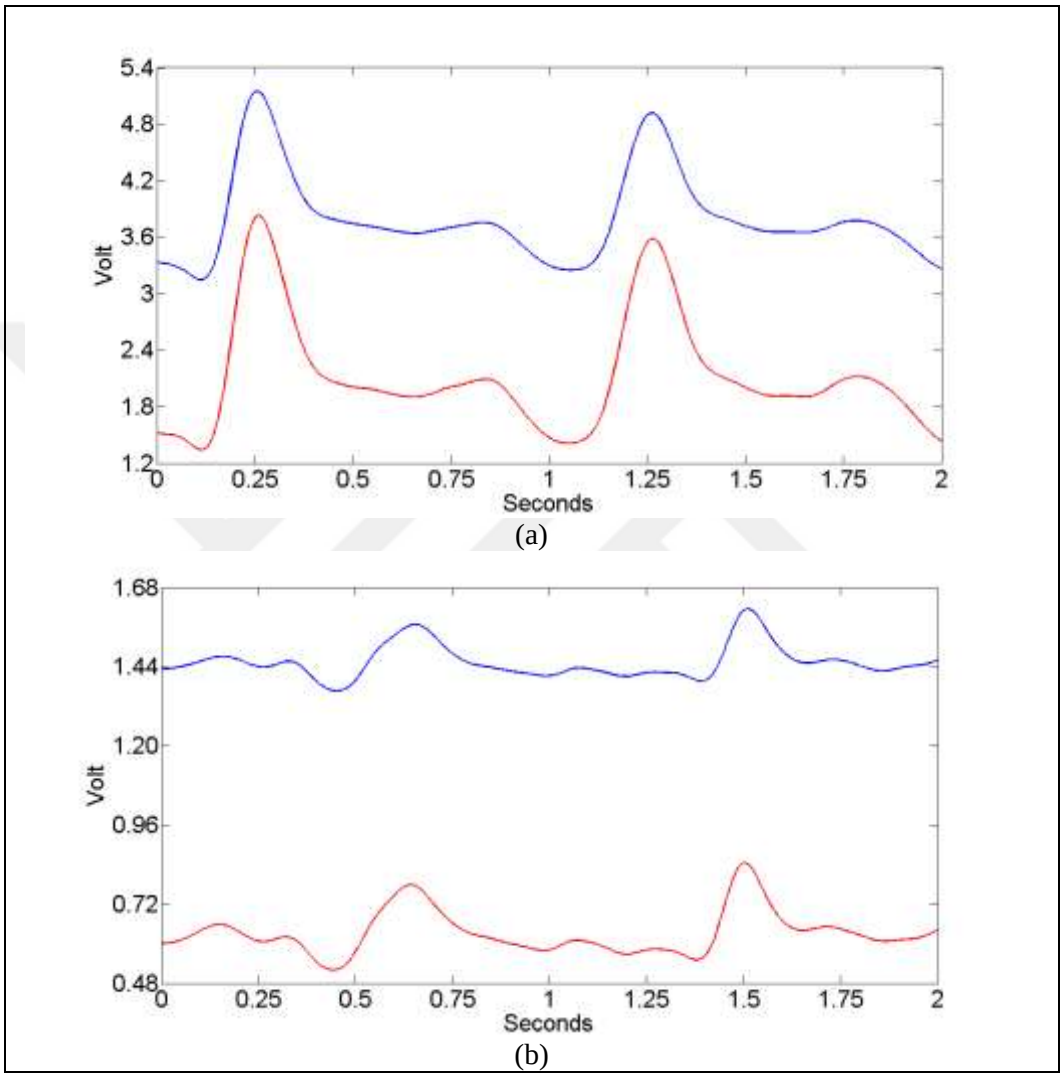

Figure 3.12. Filtered signals from a) fingertip b) chest by using Parzen-Rosenblatt window.

Table 3.6 shows the SpO_2 measurement results from the calibrated device and RR values estimated by the pulse oximeter developed in this project. The plot for those values are as seen in Figure 3.13. They are used to get the SpO_2 equation (Equitation 3.6) for Parzen-Rosenblatt window. The difference between the measurements and estimations lead to a mean error of 5.24.

Table 3.6. SpO_2 estimations from fingertip using Parzen-Rosenblatt window

Volunteers	Measured SpO_2	RR-Parzen-Rosenblatt	Estimated SpO2	Error
#1	96	0.59	101.40	5.40
#2	97	0.55	102.83	5.83
#3	96	0.67	97.98	1.98
#4	98	0.54	103.29	5.29
#5	96	0.63	99.60	3.60
#6	96	0.50	105.16	9.16
#7	97	0.64	99.14	2.14
#8	97	0.49	105.49	8.49
			Total Error	41.89
			Mean Error	5.24

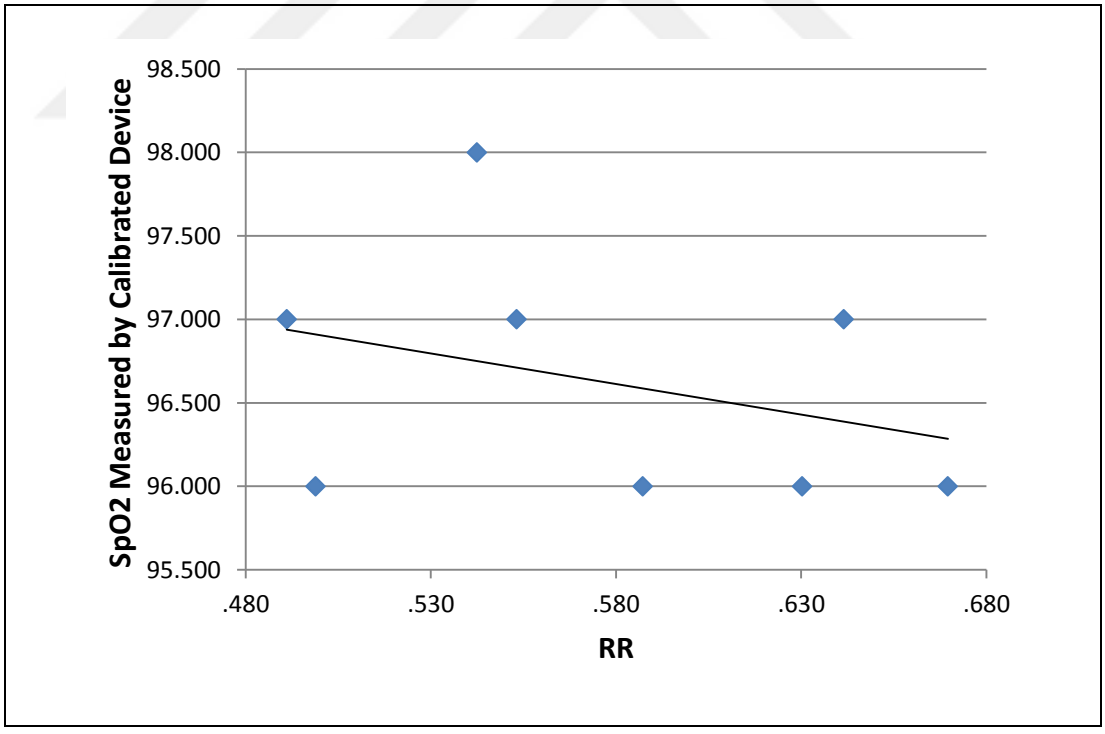

Figure 3.13. Calibration of SpO_2 estimations for Parzen-Rosenblatt window.

$$SpO_{2Parzen-Rosenblatt} = -3.66RR + 98.74 \quad (3.6)$$

Mean errors computed for Hamming, Blackman, Bartlett, DPSS, Kaiser and Parzen-Rosenblatt windows are as listed in Table 3.7. Bartlett window leads to minimum mean error for SPO2 estimations. This is due to the fact that Bartlett window adjusts the most suitable DC level for the photoplethysmogram signals.

Table 3.7. Mean Error of Digital Filtering Windows

Window Type	**Mean Error**
Hamming	4.58
Blackman	5.05
Bartlett	4.36
DPSS	5.54
Kaiser	5.6
Parzen Rosenblatt	5.24

After completing the calibration of the pulse oximeter developed in this study, Photoplethysmogram acquisitions were performed for 10 male and 11 female volunteers (mean age: 23) from right index fingertip and from the intercostal artery in the center of the left chest. Acquired signals were filtered digitally using the designed Hamming, Blackman, Bartlett, DPSS, Kaiser and Parzen-Rosenblatt windows. RR estimations were determined from the filtered signals.. The results are as tabulated in Tables 3.8, 3.9, 3.10, 3.11, 3.12 and 3.13.

The average SpO_2 estimated from chest photoplethysmogram signals are 95.87±0.26, 95.88±0.26, 95.93±30.64, 95.75±0.36, 95.84±0.32 and 95.78±0.28 for DPSS, Hamming, Kaiser, Blackman, Bartlett and Parzen-Rosenblatt windows, respectively. The average SpO_2 estimated from fingertip photoplethysmograms are 96.15±0.29, 96.15±0.25, 95.70±0.40, 96.07±0.35, 96.12±0.41 and 96.13±0.31 for DPSS, Hamming, Kaiser, Blackman, Bartlett and Parzen-Rosenblatt windows, respectively. There is no systematic difference between SpO_2 estimations from chest and from fingertip ($P < 0.5$).

Table 3.8. SpO_2 estimations for Hamming window

Volunteers	Chest		Fingertip	
	RR-Hamming	**SPO2**	**RR-Hamming**	**SPO2**
#1	0.78	95.82	0.66	96.35
#2	0.90	95.28	0.79	95.78
#3	0.74	95.99	0.72	96.08
#4	0.85	95.52	0.79	95.78
#5	0.84	95.56	0.82	95.65
#6	0.81	95.69	0.79	95.78
#7	0.78	95.83	0.73	96.04
#8	0.79	95.78	0.75	95.95
#9	0.75	95.95	0.66	96.35
#10	0.64	96.43	0.61	96.57
#11	0.82	95.67	0.63	96.48
#12	0.86	95.49	0.68	96.26
#13	0.72	96.07	0.70	96.17
#14	0.93	95.16	0.78	95.82
#15	0.76	95.91	0.76	95.91
#16	0.88	95.40	0.73	96.04
#17	0.85	95.52	0.52	96.96
#18	0.74	96.00	0.80	95.73
#19	0.74	96.01	0.68	96.26
#20	0.93	95.16	0.73	96.04
#21	0.85	96.41	0.86	95.53

Table 3.9. SpO_2 estimations for Blackman window

Volunteers	Chest		Fingertip	
	RR-Blackman	**SPO2**	**RR-Blackman**	**SPO2**
#1	0.77	95.90	0.64	96.41
#2	0.89	95.43	0.79	95.83
#3	0.73	96.06	0.72	96.12
#4	0.84	95.65	0.78	95.88
#5	0.83	95.66	0.82	95.72
#6	0.80	95.79	0.78	95.88
#7	0.77	95.92	0.73	96.06
#8	0.78	95.87	0.74	96.01
#9	0.74	96.02	0.64	96.40
#10	0.63	96.43	0.60	96.54
#11	0.80	95.79	0.62	96.48
#12	0.85	95.60	0.67	96.29
#13	0.71	96.14	0.69	96.21
#14	0.93	95.29	0.77	95.91
#15	0.77	95.91	0.75	95.98
#16	0.87	95.52	0.73	96.06
#17	0.83	95.68	0.50	96.94
#18	0.73	96.06	0.80	95.79
#19	0.73	96.06	0.67	96.29
#20	0.93	95.29	0.73	96.06
#21	0.84	96.46	0.86	95.56

Table 3.10. SpO_2 estimations for Bartlett window

Volunteers	Chest		Fingertip	
	RR-Bartlett	**SPO2**	**RR-Bartlett**	**SPO2**
#1	0.78	95.41	0.65	96.08
#2	0.90	94.81	0.79	95.37
#3	0.74	95.62	0.73	95.70
#4	0.85	95.08	0.79	95.40
#5	0.84	95.13	0.82	95.21
#6	0.81	95.26	0.79	95.39
#7	0.78	95.44	0.74	95.65
#8	0.79	95.37	0.75	95.56
#9	0.75	95.56	0.66	96.04
#10	0.64	96.12	0.62	96.25
#11	0.82	96.17	0.63	96.18
#12	0.86	96.60	0.68	95.91
#13	0.72	96.70	0.70	95.82
#14	0.93	96.76	0.78	95.41
#15	0.76	96.43	0.76	95.51
#16	0.88	96.43	0.73	95.69
#17	0.84	96.07	0.52	96.72
#18	0.74	96.07	0.80	95.35
#19	0.74	96.23	0.68	95.92
#20	0.93	97.20	0.73	95.66
#21	0.85	96.02	0.86	95.01

Tablo 3.11. SpO_2 estimations using DPSS window

Volunteers	Chest		Fingertip	
	RR-DPSS	**Estimated SPO2**	**RR-DPSS**	**Estimated SPO2**
#1	0.77	95.95	0.63	96.42
#2	0.89	95.55	0.80	95.85
#3	0.72	96.12	0.71	96.15
#4	0.83	95.75	0.77	95.95
#5	0.83	95.75	0.81	95.82
#6	0.79	95.88	0.77	95.95
#7	0.76	95.98	0.72	96.12
#8	0.77	95.95	0.74	96.05
#9	0.73	96.08	0.64	96.39
#10	0.64	96.39	0.60	96.52
#11	0.80	95.85	0.61	96.49
#12	0.85	95.68	0.66	96.32
#13	0.70	96.19	0.68	96.25
#14	0.93	95.41	0.77	95.95
#15	0.77	95.95	0.74	96.05
#16	0.87	95.61	0.74	96.05
#17	0.81	95.82	0.49	96.89
#18	0.72	96.12	0.80	95.85
#19	0.72	96.12	0.66	96.32
#20	0.93	95.41	0.73	96.08
#21	0.83	95.75	0.86	95.65

Table 3.12. SpO_2 estimations for Kaiser window

Volunteers	Chest		Fingertip	
	RR-Kaiser	**SPO2**	**RR-Kaiser**	**SPO2**
#1	0.76	95.97	0.63	96.42
#2	0.88	95.58	0.80	95.86
#3	0.72	96.11	0.71	96.16
#4	0.83	95.76	0.77	95.96
#5	0.83	95.76	0.81	95.81
#6	0.79	95.88	0.77	95.95
#7	0.76	96.00	0.72	96.13
#8	0.77	95.97	0.73	96.07
#9	0.73	96.10	0.64	96.40
#10	0.63	96.43	0.60	96.53
#11	0.79	95.88	0.61	96.50
#12	0.85	95.68	0.66	96.31
#13	0.70	96.20	0.68	96.26
#14	0.93	95.42	0.77	95.96
#15	0.77	95.95	0.74	96.06
#16	0.87	95.63	0.74	96.06
#17	0.81	95.82	0.49	96.89
#18	0.72	96.13	0.80	95.84
#19	0.72	96.13	0.66	96.33
#20	0.93	95.41	0.73	96.10
#21	0.83	95.77	0.86	95.66

Table 3.13. SpO_2 estimations for Parzen-Rosenblatt window

Volunteers	Chest		Fingertip	
	RR-Parzen-Rosenbatt	**SPO2**	**RR-Parzen-Rosenblatt**	**SPO2**
#1	0.77	95.92	0.63	96.43
#2	0.89	95.48	0.80	95.81
#3	0.73	96.06	0.71	96.14
#4	0.84	95.66	0.77	95.92
#5	0.83	95.70	0.82	95.74
#6	0.80	95.81	0.78	95.88
#7	0.76	95.95	0.72	96.10
#8	0.77	95.92	0.74	96.03
#9	0.73	96.06	0.64	96.39
#10	0.63	96.43	0.60	96.54
#11	0.80	95.81	0.61	96.50
#12	0.85	95.63	0.67	96.28
#13	0.71	96.14	0.69	96.21
#14	0.93	95.33	0.77	95.92
#15	0.77	95.92	0.75	95.99
#16	0.87	95.55	0.73	96.06
#17	0.82	95.74	0.50	96.91
#18	0.72	96.10	0.80	95.81
#19	0.72	96.10	0.66	96.32
#20	0.93	95.33	0.73	96.06
#21	0.83	95.70	0.86	95.59

4. CONCLUSION

SpO_2 value can be measured from different body locations such as fingertip, forehead, earlobe and nose. In this study, a SpO_2 measurement system was designed from chest. This system has reflectance SpO_2 sensor. SpO_2 measured from fingertip and chest to compare.

In this project, we have shown SpO_2 estimation can be taken from chest region. We have seen that results are consistent, when SpO_2 estimations are compared from fingertip and chest region.

In digital filtering, the window size for all windows is set to fifty. If the window size is increased, diastole peak of photoplethysmogram signal is lost. If the window size is decreased, artefacts could not be removed from the photoplethysmogram signal. Bartlett window leads to minimum mean error for SPO2 estimations. This is due to the fact that Bartlett window adjusts the most suitable DC level for the photoplethysmogram signals.

The device developed can be used in home care, intensive care unit, study about diagnosing detecting etc. Medical doctors agree that SpO_2 estimation should be taken from sites closer to the heart to detect some disease like hypoxia in early stage. This device achieved the closest SpO_2 measurements to the heart by this time.

The physical system was designed as a compact and low powered system, which is also comparatively cheap and reliable to be produced. The interface design is simple and easy to use, which is also compatible with many computers today and require minimal system resources to function. Due to these traits, the project is highly feasible for mass production, and a widespread use in many varieties of medical institutions.

In the future, we are planning to increase our database, trying this device to detect diagnosis. An adjustable light source with a high maximum intensity should be used in future prototypes, considering that chest area was observed to have a higher variety of hindering factors which can be overcome with a more adaptive light source and next design should be portable. Due to the time constraints, no subjects with any relevant diseases were available to take measurements from. Future studies will include a variety of

patients as test subjects, and future prototypes will be calibrated by taking these new data into consideration.

REFERENCES

1. J. B. West MD PhD. Respiratory Physiology. 2008.

2. D. Potuzakova, W. Chen, S. B. Oetomo and L. Feijs. Innovative Design for Monitoring of Neonates Using Reflectance Pulse Oximeter. *International Conference on Intelligent Environments,* pp 2107- 2113, 2011.

3. S. DeMeulenaere. Pulse Oxymetry: Uses and Limitations. *The Journal of Nurse Practitioners-JPN,* 2007.

4. R. D. Branson, D. R. Hess, R. L. Chatburn. *Respiratory Care Equipment.* Philadelphia, PA: Lippincott Williams & Wilkins, 1999.

5. S. Barker. "Motion-resistant" Pulse Oximetry: A Comparison of New and Old Models. *Anesthesia & Analgesia.* 95(4), 967-972, 2002.

6. Y. D. Lee, S. J. Jung, Y. S. Seo and W. Y. Chung. Measurement of Motion Activity during Ambulatory Using Pulse Oximeter and Triaxial Accelerometer. *Third International Conference on Convergence Hybrid Information Technology,* 2008.

7. K. Urpalainen. *Development of a Fractional Multi-Wavelength Pulse Oximetry Configuration and FPGA Technology,* 2011.

8. M. Yelderman, W. New Jr. Evaluation of Pulse-Oximetry. *Anethesiology* 59, 349-352, 1983.

9. J. W. Severinghaus. History, Status and Future of Pulse-Oximetry. *Advances in Experimental Medicine and Biology*., 220, 3-8, 1987.

10. Y. Pole.Evalution of Pulse Oximeter. *International Congress Series*, 1242,137-144, 2002.

11. S. B. Clark, R. A. Clark. Using Pulse Oximetry: A Review of Pulse Oximetry Use in Acute Care Medical Wards. *Clinical Effectiveness in Nursing*, 6, 106-110, 2002.

12. T. Aoyagi, M. Kishi, K. Yamaguchi, S. Watanabe. Improvement of an Ear-piece Oximeter. *Abreacts of the 13th Annual meeting of the Japanese Society for Medical Electronics and Biological Engineering*, JSMEBE, Osaka, Japan,90-91, 1974.

13. S. M. Tucker, M. M. Canobbio, E. V. Paquette and M. F. Wells. *Respiratory System, Patient Care Standards: Collaborative Planning and Nursing Intervention (7th Edition),* 2002.

14. D. B. MacLeod, L. I. Cortinez, J. C. Keifer, D. Cameron, D. R. Wrigth, W. D. White. The desaturation response time of finger pulse oximeter during mild hypothermia. *Anesthesia,* 60,65-71, 2005.

15. P. D. Mannheimer and D. E. Bebout. The oxiMax System: Nellcore's New Platform for Pulse Oximeter. *Minerva Anestesiologica,* 68(4), 236-239, 2002.

16. K. K. Giuliano and T. L. Higgins. New-generation Pulse Oximeter in the Care of Critically ill Patient. *American Journal of Critical Care,* 14(1), 26-39, 2005.

17. G. H. Yönt, E. A. Korhan, L. Khorshid. Comparison of Oxygen Saturation Values and Measurement Times by Pulse Oximetry in Various Parts of the Body. *Applied Nursing Research,* 2010.

18. Healthcare 4 All homepage; http://www.healthcare4all.co.uk/pulse_oximeters [retrieved 2015].

19. Lode Medical homepage; http://www.lode.nl/en/product/programmable-control-unit-with-spo2-heart-rate-1/19 [retrieved 2008].

20. The Medical World homepage: http://www.medical-world.co.uk/p/pulse-oximeters/nonin/pulse-oximeter-ear-lobe sensor/14561.

21. Covidien Medical homegape; http://www.healthymotherandbaby.com/ [retrieved 29 December 2001].

22. S. M. Park, J. Y. Kim, K. E. Ko, I. H. Jang and K. B. Sim. Real-Time Heart Rate Monitoring System based on Ring-Type Pulse Oximeter Sensor. *Journal of Electrical Engineering Technology,* Vol. 8, No. 2:376-384, 2013.

23. P. K. Baheti and H. Garudadri. An Ultra-Low Power Pulse Oximeter based on Compressed Sensing. *Wearable and Implantable Body Sensor Networks,* 144-148, 2009.

24. G. D. X. Tang and W. Liu. A Reflectance Pulse Oximeter Design Using the MSP430 F149. *International Conference on Medical Engineering,* 2007.

25. M. Nogawa, T. Kaiwa and S. Takatani. A Novel Hybrid Reflectance Pulse Oximeter Sensor with Improved Linearity and General Applicability to Various Poriton of the Body. *Proceedings of the 20th Annual International Conference of the IEEE Engineering in Medicine and Biology Society,* Vol. 20, No. 4, 1998.

26. H. Ogino, H. Minamitani and T. Souma. Reflectance Pulse Oximeter Measuring Central SaO_2 from Mouth. *Engineering in Medicine and Biology Society.* 1994, 914-915. Vol. 2.

27. C. Schreiner, P. Carterwood, J. Anderson and J. McLauglin. Blood Oxygen Level Measurement with a Chest-Based Pulse Oximetry Prototype System. *Computers in Cardiology,* 2010.

28. S. Fuke, T. Suzuki, K. Nakayama, H. Takana, S. Minami. Blood Pressure Estimation from Pulse Wave Velocity Measured on the Chest. *35th Annual International Conferences of the IEEE EMBS Osaka, Japan,* 3-7 July 2013.

29. K. A. Reddy B. George, V. J. Kumar. Use of Fourier Series Analysis for Motion Artefact Reduction an Data Compression of Photoplethysmographic Signals. *Instrumentation and Measurements*, Vol. 58, pp 1706-1711, Issue 5, 2009.

30. S. Seyedtabaii and L. Seyedtabaii. Kalman Filter Based Adaptive Reduction of Motion Artefact from Photoplethysmographic Signal. *International Journal of Electrical and Computer Engineering*, 3-9, 2008.

31. S. H. Kim, D. W. Ryoo, C. Bae. Adaptive Noise Cancellation Using Accelerometers for the PPG Signal from Forehead. *Engineering in Medicine and Biology Society, 29th Annual International Conference of the IEEE EMBS Cite Internationale*, Lyon, France, 2564-2567, 2007.

32. H. W. Lee, J. W. Lee, W. G. Jung, G. K. Lee. The Periodic Moving Average Filter for Removing Motion Artifacts from PPG Signals. *International Journal of Control, Automation, and Systems*, Vol. 5, no. 6, 701-706, 2007.

33. K. Pilk, K. Meigas, R. Ferenets, J. Kaik. Adjustment of Adaptive Sum Comb Filter for PPG Signals. *Engineering in Medicine and Biology Society, Annual International Conference of the IEEE,* Minneapolis, 5693-5696, 2009.

34. B. Lee, Y. Kee, J. Han, W. J. Yi. Adaptive Comb Filtering for Motion Artifacts Reduction from PPG with a Structure of Adaptive Lattice IIR Notch Filter. *Engineering in Medicine and Biology Society, Annual International Conference of the IEEE*, 7937-7940, Boston, 2011.

35. M. M. Ram, K. V. Madhav, E. H. Krishna, K. N. Reddy, K. A. Reddy. On the Performance of Time Varying Step-Size Least Means Squares (TVS-LMS) Adaptive Filter for MA Reduction from PPG Signals. *Communication and Signal Processing (ICCSP),* 431-435, 2011.

36. Y. K. Lee, O. W. Kwon, H. S. Shin, J. Jo, Y. Lee. Noise Reduction of PPG Signal Using a Particle Filter for Robust Emotion Recognition. *IEEE International Conference on Consumer Electronics*, Berlin 202-205, 2011.

37. Y. Yuliang, X. Lin, Z. Lulu, C. Yang, W. Meng. PPG Signals Processing Using Wavelet Transform and Adaptive Filter. *32nd Control Conference (CCC)*, Chine, 3623-3627, 2013.

38. K. V. P. Naraharisetti, M. Bawa, M. Tahernezhadi. Comparison of Different Signal Processing Methods for Reducing Artifacts from Photoplethysmogram Signal. *IEEE International Conference on Electro/International Technology.* 1-8, 2011.

39. J. E. Scharf, S. Athan and D. Cain. Pulse Oximetry Through Spectral Analysis. *Biomedical Engineering Conference*, 227-229, 1993.

40. E. M. Lee, N. H. Kim, N. T. Trang, J. H. Hong, E. J. Cha and T. S. Lee. Respiratory rate Detection Algorithms by Photoplethysmographic Signal Processing. *Engineering in Medicine and Biology Society.* 20-25, 2008.

41. B. Becerra-Luna, J. C. Sanchez, R. Martinez-Memije and O. Infante. Photopletysmographic Fingertip with Miokinetic Noise Attenuation Using an Accelerometer and Adaptive Filtering Technique. *Health Care Exchanges (PAHCE) 2013 Pan America*, 1-5, 2013.

42. Y. H. Yang, K. T. Tang. A Pulse Oximetry System with Motion Artifact Reduction Based on Fourier Analysis. *International Symposium on Bioelectronics and Bioinformatics*, 1-4, 2014.

43. K. Safgat, D. P. Jones. R. M. Langford and P. A. Kyriacou. Filtering Techniques for the Removal of the Ventilator Artefacts in Oesophageal Pulse Oximetry. *Medical and Biological Engineering and Computing,* DOI 10.1007/s11517-006 -0089-2, 44:729-737, 2006.

44. Y. Dai and J. Luo. Design of Noninvasive Pulse Oximeter Based on Bluetooth 4.0 BLE. *Seventh Symposium on Computational Intelligence and Design (ISCID)*, Vol. 1, 100-103, 2014.

45. D. Kollman, W. K. Hogan, C. Steidl, M. K. Hibbs-Brenner, D. S. Hedin, P. A. Lichter. VCSEL Based, Wearable, Continuously Monitoring Pulse Oximeter. *Engineering in Medicine and Biology Society*, 4156-4159, 2013.

46. K. Li and S. Warren. A Wireless Reflectance Pulse Oximeter With Digital Baseline Control for Unfiltered Photoplethysmograms. *Biomedical Circuits and Systems,* Vol 6, Issue 3, 269-278, 2011.

47. G. Ateş and K. Polat. Measuring of Oxygen Saturation Using Pulse Oximeter Based on Fuzzy Logic. *International Symposium on Medical Measurements and Applications Proceedings.* 1-6, 2013, ISBN: 978-1-4673-0880-9.

48. C. L. Peterson, G. Heng, M. J. Maclnnis, G. A. Dumont, J. M. Ansermino. Ultra-low-cost Clinical Pulse Oximetry. *35th Annual International Conference of the Engineering in Medicine and Biology Society,* 2874- 2877, 2013.

49. J. P. de Kock, L. Tarasenko, C. J. Glynn, A. R. Hill. Reflectance Pulse Oximetry Measurements from the Retinal Fundus. *Transection on Biomedical Engineering,* Vol. 40, Issue 8, 817-823, 2002.

50. D. Potuzakova, W. Chen, S. B. Oetomo and L. Feijs. Innovative Design for Monitoring of Neonates Using Reflectance Pulse Oximeter. *International Conference on Intelligent Environments*, 2107- 2113, 2011.

51. J. W. Nilsson and S. A. Riedel. “Electric Circuit”, Eighth Edition, 2008.

52. R. D. Branson, D. R. Hess, R. L. Chatburn. *Respiratory Care Equipment.* Philadelphia, PA: Lippincott Williams & Wilkins, 1999.

53. Vishay Semiconductors. Silicon NPN Phototransistor, RoHS Compliant. 2008.

54. RM42L432 16 and 32 Bit RISC Flash Microcontroller, Texas Instrument, 2013.

55. Texas Instrument LMx58-N Low-Power, Dual-Operational Amplifier Datasheet, homepage: http://www.ti.com/lit/ds/symlink/lm158-n.pdf [retrieved December 2014].

56. A. H. Nuttall. Some Windows with Very Good Side lobe Behavior. *IEEE Transaction on Acoustics, Speech, Signal Processing,* vol. ASSP-19, 84-91, 1981.

57. R. B. Blackman and J. W. Tukey. The Measurement of Spectra. *New York :Dover,* 1958, appendix B.5, 95-100.

58. D. Slepian and H. Pollak. Prolate-speroidal Wave Functions, Fourier Analysis and Uncertainity-- i. *Bell System Technical Journal,* vol 40,. 34-64 , 1961.

59. F.J. Harris. On the Use of Windows for Harmonic Analysis with the Discrete Fourier Transform. *Proceedings of IEEE,* Vol. 66, 51-83, 1978.

60. J.F. Kaiser. Using the I_0-Sinh Window Function. *IEEE Transactions on Circuits Systems: Fundamentals Theory and Applications,* 20-23, 1974.

61. M. Rosenbatt. Remarks on Some Nonparametric Estimates of a Density Function. *Annals of Mathematical Statistics,* Vol. 27, Issue 3, 832-837, 1956.

62. E. Parzen. On Estimation of a Probability Density Function and Mode. *Annals of Mathematical Statistics.* Vol. 33, Issue 3, 1065-1076, 1962.7.

63. Permed homepage: http://www.permed.com.br/oximetro-de-pulso-palplus-1-sa210-rossmax~324~27~2~equipamentos~oximetros.

64. N. Stuban, N. Masatsugu. Non- invasive Calibration Method for Pulse Oximeter. *Periodica Politechnica,* 52/1.2, 91-94, 2008.